



Faculty of Engineering

**REVIEW: SYNTHESIS OF STARCH BASED AEROGELS VIA  
AMBIENT PRESSURE DRYING**

**MOHD HARITH BIN RAMZI**

**Bachelor of Engineering with Honors  
(Mechanical and Manufacturing Engineering)  
2020**

# **SYNTHESIS OF STARCH BASED AEROGELS**

**MOHD HARITH BIN RAMZI**

A thesis submitted in partial fulfilment  
of the requirement for the degree of  
Bachelor of Engineering with Honors  
(Mechanical and Manufacturing Engineering)

Faculty of Engineering  
Universiti Malaysia Sarawak

2020

UNIVERSITI MALAYSIA SARAWAK

Grade: \_\_\_\_\_

Please tick (✓)

Final Year Project Report

Masters

PhD

DECLARATION OF ORIGINAL WORK

This declaration is made on the 29<sup>th</sup> day of August 2020.

**Student's Declaration:**

I **MOHD HARITH BIN RAMZI, 58751** from **FACULTY OF ENGINEERING** hereby declare that the work entitled **REVIEW: SYNTHESIS OF STARCH BASED AEROGELS VIA AMBIENT PRESSURE DRYING** is my original work. I have not copied from any other students' work or from any other sources except where due reference or acknowledgement is made explicitly in the text, nor has any part been written for me by another person.

29.07.2020

\_\_\_\_\_  
Date submitted



\_\_\_\_\_  
MOHD HARITH BIN RAMZI (58751)

**Supervisor's Declaration:**

I **DR MAHSURI BINTI YUSOF** hereby certifies that the work entitled **REVIEW: SYNTHESIS OF STARCH BASED AEROGELS VIA AMBIENT PRESSURE DRYING** was prepared by the above named student, and was submitted to the "FACULTY" as a \* partial/full fulfillment for the conferment of **BACHELOR OF ENGINEERING WITH HONOURS (MECHANICAL AND MANUFACTURING ENGINEERING)**, and the aforementioned work, to the best of my knowledge, is the said student's work.

Received for examination by: \_\_\_\_\_

**DR MAHSURI BINTI YUSOF**

Date: \_\_\_\_\_

I declare that Project/Thesis is classified as (Please tick (√)):

**CONFIDENTIAL** (Contains confidential information under the Official Secret Act 1972)\*

**RESTRICTED** (Contains restricted information as specified by the organisation where research was done)\*

**OPEN ACCESS**

### Validation of Project/Thesis

I therefore duly affirmed with free consent and willingness declare that this said Project/Thesis shall be placed officially in the Centre for Academic Information Services with the abiding interest and rights as follows:

- This Project/Thesis is the sole legal property of Universiti Malaysia Sarawak (UNIMAS).
- The Centre for Academic Information Services has the lawful right to make copies for the purpose of academic and research only and not for other purpose.
- The Centre for Academic Information Services has the lawful right to digitalise the content for the Local Content Database.
- The Centre for Academic Information Services has the lawful right to make copies of the Project/Thesis for academic exchange between Higher Learning Institute.
- No dispute or any claim shall arise from the student itself neither third party on this Project/Thesis once it becomes the sole property of UNIMAS.
- This Project/Thesis or any material, data and information related to it shall not be distributed, published or disclosed to any party by the student except with UNIMAS permission.

Student signature \_\_\_\_\_

(29.07.2020)

Supervisor signature: \_\_\_\_\_

( )

Current Address:

**LOT 2688, FASA 1, KAMPUNG ASSYAKIRIN, 97000 BINTULU SARAWAK, MALAYSIA**

Notes: \* If the Project/Thesis is **CONFIDENTIAL** or **RESTRICTED**, please attach together as annexure a letter from the organisation with the period and reasons of confidentiality and restriction.

[The instrument is duly prepared by The Centre for Academic Information Services]

# ACKNOWLEDGEMENT

All praise to Allah SWT for His blessings and giving me the strength to complete the thesis successfully. Without His righteousness, I would not be able to achieve what I currently have. First and foremost, I would like to express my deepest appreciation to my beloved supervisor, Dr Mahsuri Yusof who has the essence of a genius; she continually and convincingly conveyed a spirit of adventure in regard to research and an excitement to teaching. Without her guidance and persistent help, this thesis would not have been possible. Above ground, I am indebted to my parents and family whose value to me only grows with age. Moreover, I would like to extend my immense gratitude to my friends as their presence and support was very meaningful and important in a process that is often felt as tremendously solitaire. The love and attentiveness that I have received are overwhelming yet I am forever grateful.

# ABSTRACT

Porous material made from biomaterial like aerogels has been getting numerous attentions in the research arena lately. Aerogel is classified as a material of light weight and open pores accompanied with high specific surface area. Starch based aerogels are a class of advanced biomaterial made in the same way as bio-aerogels based on other polysaccharides via starch gelatinization, retrogradation, organic solvent exchange, and process of drying. Essentially, there are three most common drying mechanism of aerogel available which are supercritical carbon dioxide drying, freeze drying and ambient pressure drying. This paper reviews the potential outcome of synthesis of starch aerogel via ambient pressure drying based on similar studies conducted previously. This review summarizes the potential functional properties of starch-based aerogel based on similar polysaccharide aerogels like cellulose and chitosan aerogels which were synthesized via ambient pressure drying. Comparative analysis between similar porous materials was executed to reveal any advantages of the former. Thus, through this detailed review on previous polysaccharide aerogels despite having limited studies on starch-based aerogel via ambient pressure drying, the expected result of starch-based aerogel synthesized via this route can be forecasted. This paper analyses essential properties of starch-based aerogel reflected through this processing route such as morphology and microstructure, density and shrinkage, mechanical properties and thermal conductivity of the material. There are numerous ways to achieve variety of morphology and properties by varying the preparation condition to yield varying results tunable to the desired application. Therefore, with chemical and physical modification open up the possibilities of wide range of aerogels' properties and applications.

# ABSTRAK

Bahan berpori yang terbuat dari bahan bio seperti *aerogel* telah mendapat perhatian di arena penyelidikan akhir-akhir ini. *Aerogel* diklasifikasikan sebagai bahan ringan dan mempunyai liang terbuka disertai dengan jumlah luas permukaan yang tinggi. *Aerogel* berasaskan kanji adalah dalam kategori bahan bio yang canggih yang dibuat dengan cara yang sama seperti *bio-aerogel* berdasarkan polisakarida lain melalui gelatinisasi kanji, retrogradasi, pertukaran pelarut organik, dan proses pengeringan. Pada dasarnya, terdapat tiga mekanisme pengeringan *aerogel* seperti pengeringan karbon dioksida superkritik, pengeringan beku dan pengeringan tekanan ambien. Makalah ini mengkaji kemungkinan hasil sintesis *aerogel* berasaskan kanji melalui pengeringan tekanan ambien berdasarkan kajian serupa yang dilakukan sebelumnya. Ulasan ini meringkaskan potensi kemampuan berfungsi *aerogel* berasaskan kanji berdasarkan *aerogel* polisakarida yang serupa seperti *aerogel* selulosa dan citosan yang disintesis melalui pengeringan tekanan ambien. Analisis perbandingan antara bahan berliang yang serupa dilakukan untuk melihat beberapa kelebihan yang penting pada struktur ini. Oleh itu, tinjauan terperinci berdasarkan kajian yang terdahulu terhadap penghasilan aerogel berasaskan kanji melalui proses pengeringan boleh membantu kita meramal struktur yang terhasil. Makalah ini menganalisis beberapa sifat penting *aerogel* berasaskan kanji seperti morfologi dan struktur mikro, ketumpatan dan pengecutan, sifat mekanik dan kekonduksian haba bahan. Terdapat banyak teknik untuk menghasilkan pelbagai morfologi dan sifat seperti dengan mempelbagaikan keadaan persekitaran sebelum pemrosesan hingga sehingga proses selesai. Faktor tersebut akan menghasilkan sifat produk yang berbeza. Pengubahsuaian kimia dan fizikal mampu menghasilkan aerogel yang mempunyai pelbagai sifat dan seterusnya menjurus kepada kepelbagaian aplikasi *aerogel*.

# TABLE OF CONTENTS

<b>LIST OF TABLES .....</b>	<b>iii</b>
<b>LIST OF FIGURES .....</b>	<b>iv</b>
<b>LIST OF SYMBOLS .....</b>	<b>vi</b>
<b>LIST OF ABBREVIATIONS .....</b>	<b>vi</b>
<b>CHAPTER 1 INTRODUCTION .....</b>	<b>1</b>
1.1 Background .....	1
1.2 Problem Statement .....	2
1.3 Objectives .....	2
1.4 Research Scope .....	3
1.5 Thesis Outline .....	3
<b>CHAPTER 2 LITERATURE REVIEW .....</b>	<b>4</b>
2.1 Introduction .....	4
2.2 Types of Aerogels and Application .....	4
2.3 Hydrophobic and Hydrophilic Aerogels .....	5
2.4 Synthesis of Aerogels .....	7
2.4.1 Sol Gel Process .....	7
2.4.2 Advantages of Sol Gel .....	10
2.5 Property of Aerogels .....	10
2.6 Biodegradable Aerogels .....	11
2.7 Cellulose Aerogels .....	11
2.7.1 Preparation of Cellulose Aerogels .....	12
2.7.2 Properties of Cellulose Aerogels .....	14
2.8 Starch Aerogels .....	14
2.8.1 Properties of Starch Aerogels .....	15



2.8.2 Morphology of Starch Aerogels.....	16
2.8.3 Thermal Properties of Starch Aerogels.....	17
2.8.4 Production of Starch Aerogels.....	18
2.8.5 Various Application of Starch Aerogels.....	22
2.9 Executive Summary.....	24
<b>CHAPTER 3 METHODOLOGY.....</b>	<b>25</b>
3.1 Introduction.....	25
3.2 Materials.....	25
3.3 Synthesis of Starch Aerogels.....	25
3.3.1 Hydrogel Formation.....	26
3.3.2 Solvent Exchange and Esterification.....	26
3.3.3 Ambient Pressure Drying.....	27
3.4 Sample Characterization.....	29
3.4.1 Scanning Electron Microscopy.....	29
3.4.2 Density Measurement.....	29
3.4.3 Thermal Conductivity Test.....	30
<b>CHAPTER 4 EXPECTED RESULT AND DISCUSSION.....</b>	<b>34</b>
4.1 Introduction.....	34
4.2 Structural, physicochemical and functional properties of wheat starch-based aerogels.....	34
4.2.1 Effect of drying technique: Ambient pressure drying.....	34
4.2.2 Density and shrinkage.....	43
4.2.3 Mechanical properties of wheat starch aerogels.....	49
4.2.4 Thermal Conductivity of Starch-based Aerogel.....	55
<b>CHAPTER 5 CONCLUSION AND FUTURE RESEARCH DIRECTION.....</b>	<b>60</b>
<b>QUESTIONS AND ANSWERS.....</b>	<b>62</b>
<b>REFERENCES.....</b>	<b>63</b>
<b>APPENDIX.....</b>	<b>72</b>

# LIST OF TABLES

Table 2.1 Past researches on the production of starch aerogels .....	18
Table 2.2 Various application of starch aerogels .....	22
Table 3.1 TM3030 specification .....	29
Table 4.1 Density of several types of aerogel dried via different drying techniques .....	48
Table 4.2 Summary of mechanical properties of cellulose materials (Ganesan et al., 2016) ..	50
Table 4.3 Physical and textural properties of silica with different content of ATP fibers (Li et al., 2017) .....	57
Table 4.4 Thermal conductivity of several types of aerogel dried via different drying techniques .....	58

# LIST OF FIGURES

Figure 2.1 The schematic diagram for hydrophilic silica aerogels .....	6
Figure 2.2 The schematic diagram for hydrophobic silica aerogels .....	6
Figure 2.3 Steps to synthesizing aerogels (Błaszczński et al., 2013) .....	8
Figure 2.4 Preparation and application of cellulose aerogels (Long et al., 2018) .....	12
Figure 3.1 Schematic diagram of processing steps to synthesize starch aerogels (Ubeyitogullari & Ciftci, 2016) .....	26
Figure 3.2 Flowchart for the formation of wheat starch-based aerogel .....	28
Figure 3.3 Experimental set up outline (PA Hilton H112A Manual) .....	30
Figure 3.4 Temperature measurement outline (PA Hilton H112A Manual) .....	31
Figure 3.5 The position of the hydrogel sample inside the heat conduction unit .....	31
Figure 4.1 Pictures of hydrogel, alcogel, aerogel and xerogel derived from wheat starch (Ubeyitogullari & Ciftci, 2016) .....	35
Figure 4.2 The stress analysis of pore walls of porous materials during the drying process and (b) schematics of the cross-linked networks (Y. Li et al., 2019). .....	36
Figure 4.3 SEM images of chitosan-urea gels (a) SCD aerogel (30'000x) (b) APD aerogel (30'000x) (c) SCD aerogel (100'000x) (d) APD aerogel (100'000x) SCD and APD images are from gels prepared from a 5% m/v and 10% m/v chitosan solution, respectively (Guerrero- Albuquerque et al., 2020) .....	37
Figure 4.4 Nitrogen sorption data (a) Nitrogen sorption isotherms of 10% chitosan sample (b) BJH desorption plots of 10% chitosan sample (c) Surface area as a function of density for all different chitosan concentrations (Guerrero-Albuquerque et al., 2020). .....	38
Figure 4.5 The SEM images of cross-sectioned xerogels of cellulose scaffolds obtained from the solvent medium; isopropanol (a and b) and ethanol (c and d) (Ganesan et al., 2016) .....	39
Figure 4.6 BET specific surface areas of the aerogel composites. Dashed line corresponds to the theoretical specific surface area (details in text) (Markevicius et al., 2017) .....	40
Figure 4.7 SEM images of silica phase in supercritical dried (a) and ambient-dried (b) composite aerogels (Markevicius et al., 2017) .....	41
Figure 4.8 (a-c) SEM images of freeze dried cellulose aerogels (d-f) SEM images of atmospheric dried cellulose aerogels (g) Nitrogen adsorption and desorption isotherms and	

(h) Barret-Joyner-Halenda (BJH) pore size distribution of cellulose aerogel prepared with freeze drying method (blue) and atmospheric pressure drying method (red) (Li et al., 2019). .....	42
Figure 4.9 (a) Linear shrinkage as a function of chitosan concentration (b) Density dependence on chitosan concentration (c) Thermal conductivity versus chitosan concentration (d) Thermal conductivity versus density (Guerrero-Alburquerque et al., 2020) .....	45
Figure 4.10 Physical Properties; density (g/cm <sup>3</sup> ) of wheat starch aerogel monoliths at different gelatinization temperatures and starch concentrations with a mixing rate of 600 rpm (Ubeyitogullari & Ciftci, 2016) .....	46
Figure 4.11 Total sample shrinkage as a function of fiber weight fraction for ambient-dried and supercritical-dried aerogels (Monolithic ambient-dried aerogel without addition of fibers is not possible; therefore, the shrinkage of this sample was not determined) (Markevicius et al., 2017). .....	47
Figure 4.12 The stress-strain curve of cellulose scaffolds (Ganesan et al., 2016).....	51
Figure 4.13 The stress-strain curves at 25°C of (a) the starch-enhanced melamine-formaldehyde (SEMF) aerogel and (b) pure melamine-formaldehyde (MF) aerogel (Zhang et al., 2017). .....	52
Figure 4.14 (a) Compression strain-stress of cellulose aerogels prepared with freeze drying method and ambient pressure drying (b) 5 cyclic fatigue compression strain-stress test with a compression of 50% (Li et al., 2019).....	54
Figure 4.15 Thermal conductivity of Tencel fiber-silica composite aerogels prepared via ambient pressure drying and supercritical drying (Markevicius et al., 2017) .....	56
Figure 4.16 The effect of fiber content on thermal conductivity of the ATP/silica aerogel composite (Li et al., 2017) .....	58

## LIST OF SYMBOLS

W	Watts
K	Thermal Conductivity
°C	Celcius
Q	Heat Flow
$\rho$	Density
m	Mass
V	Volume

## LIST OF ABBREVIATIONS

APD	Ambient Pressure Drying
SCD	Supercritical Drying
FD	Freeze Drying
ASTM	American Standard Test Methods
SEM	Scanning Electron Microscopy
BET	Brunauer–Emmet–Teller
BJH	Barret–Joyner–Halenda
CNF	Cellulose Nanofibrils
PMSQ	Polymethylsilsesquioxane
TMCS	Trimethylchlorosilane

# CHAPTER 1

## INTRODUCTION

### 1.1 Background

The popularity of aerogels is increasing and continue growing over the years due to its amazing properties and various applications ranging from home to space applications. Today, there are various types of aerogels such as silica aerogels, cellulose aerogels, oxide aerogels and alumina and other oxide aerogels. According to Koh et al. (2018), aerogels are lightweight materials with low densities  $\left(0.003 - 0.5 \frac{g}{cm^3}\right)$ , low thermal conductivities (0.005 – 0.045 W/m·K) and high porosity. Due to this mechanical properties and its versatility, aerogels are widely used for various technical applications laser experiments, ultrasonic and gas sensors, nuclear particle detection, thermal insulation, waste management gas absorption, radioactive waste confinement, optics and light-guides, electronic devices, energy storage, imaging devices, catalysts and X-ray laser research (Hrubesh, 1998)

Starch is a promising source of aerogel formation at low cost, sustainable, abundant and bio-based (Ubeyitogullari & Ciftci, 2016). According to Maningat et al. (2009), among various starch sources, wheat starch is the world's third most produced type of starch which has the potential to form three dimensional polymeric network structures of starch hydrogels whilst playing a crucial role in food. Maningat et al. (2009) further explained that wheat starch has a composition of 25% amylose and 75% amylopectin.

To date, wheat starch has restricted usage and application which is mainly for the production flour (Ubeyitogullari & Ciftci, 2016). In the recent years, various materials have been used to develop aerogels with enhance properties which includes corn starch (García-González et al., 2015; Kenar et al., 2014) and hybrid (composed of inorganic and organic combination) materials such as silica-cellulose (Demilecamps et al., 2015).

## **1.2 Problem Statement**

Generally, aerogels exhibit countless of outstanding properties which often leads to their potential application in various fields. In a manufacturing study conducted by Dorcheh and Abbasi (2008), the production of silica aerogel utilizes toxic chemicals, high consumption of solvent in their diffusion-controlled processes and high pressure vessels running for an extended period of time depending on the drying process.

According to Long et al. (2018), the precursors of synthetic polymer-based aerogels are non-degradable and toxic. In another study conducted by Filipe (2015) stated that the production of inorganic aerogels (from extraction of raw materials to production phase) in comparison with monolithic hybrid aerogels posed the highest environmental impact in terms of abiotic depletion, photochemical oxidation and global warming photochemical oxidation indicators.

Therefore, it is safe to deduce that a more environmental-friendly and greener approach to synthesize aerogels derived from organic source is highly demanded to replace the existing conventional methods.

## **1.3 Objectives**

The objectives of this study are stated as follows;

- i. To review the synthesis starch-based aerogels via ambient pressure drying (APD),
- ii. To review the morphology and microstructures of starch-based aerogels of different starch concentrations in the dispersion, the gelatinization temperature, the incorporation of non-starch material (as cross-linking agents), the incorporation of surface modification agents and the drying temperature, and
- iii. To review the physical properties of starch-based aerogels of different starch concentrations in the dispersion, the gelatinization temperature, the incorporation of non-starch material (as cross-linking agents), the incorporation of surface modification agents and the drying temperature.

## **1.4 Research Scope**

Wheat starch is used as the source of starch to synthesize the starch-based aerogels. Ambient pressure drying (APD) is used as the mechanism to dry the aerogels. A scanning electron microscope is used to carry out the micrography analysis.

## **1.5 Thesis Outline**

This thesis is divided into five chapters which comprise of the overall details of the review paper. In Chapter 1, the introduction of the review is explained by clarifying the background, problem statements, objectives and the scopes of the proposed methodology.

Moreover, Chapter 2 elaborates on the literature review of the paper. In this chapter, concepts and findings of a particular field related to the review are clarified. The general concept of aerogels is explained with an overview of aerogels and types of aerogels. The synthesis and method to produce aerogels based on previous studies are also included in this review paper. The available methods to produce aerogels are supplemented with the properties of aerogels and the wide range of application.

Chapter 3 focuses on the proposed methodology of the project. The methodology is briefly illustrated in a flowchart supplemented in this chapter to explain on the planning and organizing process of executing the project. This chapter is also accompanied by the characterization methods of samples to obtain the results. The calculation for the concerned parameter is also included as to cover the detailed explanation of the matter.

Moreover, Chapter 4 showcases the expected result and discussion of starch-based aerogel. A collective result from previous studies of similar scopes and spectrum is used to achieve consistency in result expectation and forecast. The highlighted parameters include the morphology and microstructure of aerogels, density and shrinkage, mechanical properties and finally thermal conductivity of aerogels.

Lastly, Chapter 5 provides the overall conclusion and future research direction of this study. This section emphasizes on the expected outcomes and provide structured research direction for further works in the recurring field of study.



# CHAPTER 2

## LITERATURE REVIEW

### 2.1 Introduction

This chapter reviews the types of aerogels exist in the commercial market today and its various commercial and technical applications. This chapter will also review the synthesis of aerogels, mechanical properties of aerogels and biodegradable aerogels.

### 2.2 Types of Aerogels and Application

There are three types of aerogels commonly found which includes silica, carbon and metal oxides. In practical applications, the most common among the three types of aerogels is the silica aerogel. This is because silica aerogels exhibit amazing properties which opens to windows of many potential applications.

The pilot production of silica aerogels started in 1930s, but saw little development for several decades (Soleimani et al., 2008). Silica aerogels has found its way in many commercial applications. One of the most interesting commercial application of silica aerogels include molds for casting aluminum metal, wastewater treatment, heat storage device for automobiles (Ahmed & Attia, 1995; Alkemper et al., 1995; Herrmann et al., 1995). It was also reported that silica aerogel are involved in the application of transparent window components, building walls transparent heat insulator or vacuum insulation (Herrmann et al., 1995).

Another type of aerogels is carbon aerogels. Carbon aerogels are considered as a very promising type of materials for various energy related applications due to their high mass-specific surface area and electrical conductivity, environment benignity and inertness of chemical (Biener et al., 2011). It has been reported that a recent developed carbon aerogels

with a new class of ultra-high surface area are used as hydrogen physisorbents (Kabbour et al., 2006). A process called thermal activation is used to prepare this material at which involving the controlled incineration of carbon from aerogel structure in an oxidizing atmosphere like carbon dioxide (Biener et al., 2011). Biener et al. (2011) also reported that through the carbon removal, new micropores are created within the microstructures and thus resulted in the increment of overall surface area. Another application of carbon aerogels is in the field of green technologies as electrical double-layer capacitor, EDLC (Pekala et al., 1998). It was reported that in the device, the storage of the charge was in the form of ions amassed on the surface of the material and subsequently resulted in the formation of a midway between electrostatic capacitors and batteries (Conway, 1991). Beyond its application as energy storage, carbon aerogels are also used to boost the performance of other solid-state hydrogen storage materials especially multifaceted hybrids (Biener et al., 2011). Biener et al. (2011) also reported that carbon aerogels is one of the most potential candidates for this application due to their tunable porosities, oversized pore volumes and its ability to adjust the surface characteristics of the carbon framework.

Metal oxide aerogels can be classified as inorganic cousins of silica aerogels which exhibits their own unique properties. This type of aerogels are very interesting nonporous materials used the application of thermal insulations, catalysts, sensors and etc. Examples of metal oxide aerogels includes Iron Oxide, Zirconia, Titania, Alumina, Chromia and Vandia. Some applications of various metal oxide aerogels includes filtration, sorption media or photocatalysts, in medical or electrochemical and optical application (Feinle & Hüsing, 2015).

### **2.3 Hydrophobic and Hydrophilic Aerogels**

In the present market today, there are two existing types of aerogels which can be categorized as hydrophobic and hydrophilic aerogels. The following text will be only for silica hydrophobic and hydrophilic aerogels. Figure 2.1 and Figure 2.2 show the schematic diagram of hydrophilic silica aerogels and hydrophobic silica aerogels, respectively.

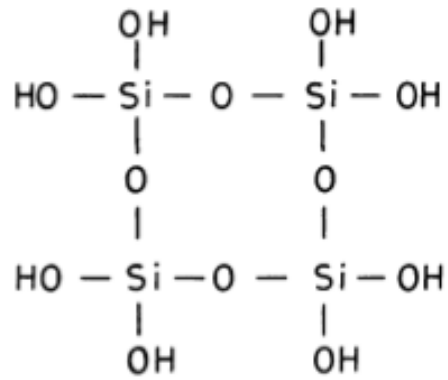


Figure 2.1 The schematic diagram for hydrophilic silica aerogels

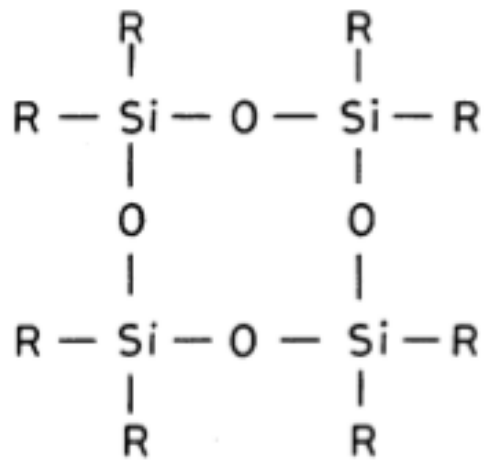


Figure 2.2 The schematic diagram for hydrophobic silica aerogels

The aerogel's hydrophobicity originates from the chemical structure of the aerogel. The main source of hydrophilicity of the aerogel is the Si-OH structure as this particular chemical structure promotes the adsorption of water (Wagh & Ingale, 2002). Wagh and Ingale (2002) also further clarified that when a hydrolytically stable Si-R (R=CH<sub>3</sub>) replaces the Si-OH structure, the aerogel will exhibit hydrophobicity as it prevents the water adsorption and will not be susceptible to water.

There are two methods to achieve hydrophobic aerogels namely (a) surface chemical modification of aerogels by gaseous reagents and (b) surface modification of the colloidal particles by the incorporation of certain hydrophobic reagents in the alcohol.

## 2.4 Synthesis of Aerogels

### 2.4.1 Sol Gel Process

There are two critical steps involved in preparation of aerogels. The first step is called a sol-gel process to form the gel followed by the second step which is the drying process to obtain the aerogel (Bangi et al., 2018). Bangi et al. (2018) also stated the fundamental step to synthesizing the aerogels is the sol-gel process which takes place via hydrolysis and polycondensation of precursor solutions to form gels. ‘The process of dispersion of nanoparticles in the liquid phase is called sol whilst the result of this process which leads to the aggregation to form a continuous three dimensional network is called gel (da Silva et al., 1992). The synthesis of aerogel through the sol-gel method can be categorized into a series of steps and depicted as in Figure 2.3 (Błaszczyszki et al., 2013). The steps to synthesizing aerogels is shown in Figure 2.3.

**Step 1:** Formation of alkoxide or solvated metal precursor (sol).

**Step 2:** Polycondensation reactions to result in gelation (rapid viscosity increments of the solution) from an oxide- or alcohol bridged network (gel).

**Step 3:** Gelatinization; polycondensation reactions continue until the gel forms a solid mass, followed by contraction of gel network and removal of solvent from gel pores.

**Step 4:** This step involves shaping of the gel accompanied by the drying process. The manner solvent removal process dictates the porosity of the end material.

There are three known methods of drying aerogels which includes super critical drying (SCD), ambient pressure drying (APD) and freeze drying (FD). According to Bangi et al. (2018), SCD is a drying method which utilizes the drying of present liquid in the pores of the gel above the critical pressure and temperature while APD is a drying process which only uses the ambient pressure and temperature above 150 °C. Bangi et al. (2018) further elaborated that FD is a drying process of the frozen gel in a vacuum.

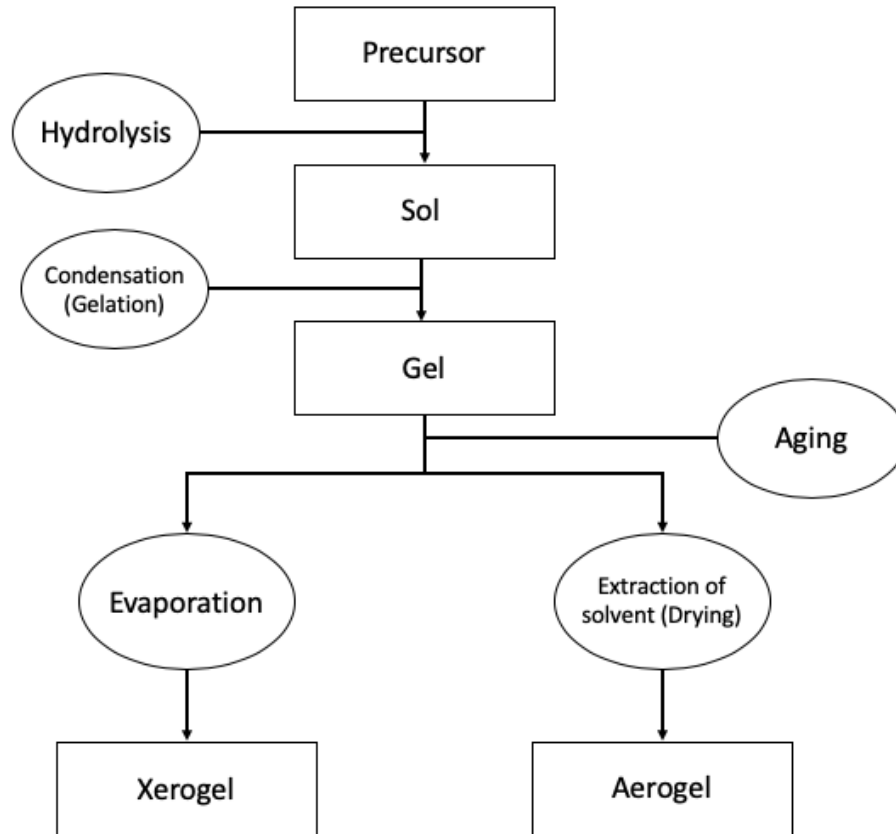


Figure 2.3 Steps to Synthesizing Aerogels (Błaszczyszński et al., 2013)

SCD is a conventional way of aerogel drying process. It was first performed in 1931 by Kistler at Stanford University using sodium silicate ( $\text{Na}_2\text{SiO}_3$ ) as a starting material (Kistler, 1931). This conventional drying method is then often used. This drying method is also frequently used in the process of drying the three dimensional scaffolds for the maintenance of macro- and nano- hydrogel structure (García-González et al., 2012). García-González et al. (2012) inferred that this approach does not lead to surface tension and vapor-liquid transition. This is due to the ability of this process to prevent the shrinkage of the porous structure (Yan et al., 2019). Yan et al. (2019), also further elaborate this process often comes with a high production cost which includes high equipment requirement, high energy usage and heavy operating hazard. Super critical drying involves a systematic solvent exchange to any solvent that are miscible with carbon dioxide such as acetone and ethanol (Darpentigny et al., 2019). Darpentigny et al. (2019) further elaborated that the process of solvent exchange with liquid carbon dioxide usually takes place at low

temperatures and high-pressure prior achieving the supercritical state. Mild supercritical parameters of temperatures

APD is another method of aerogel drying process. This method is capable for large-scale application due to its advantages of simple operation and high safety (Rao et al., 2007). However, the conventional process of APD is tedious as it involves solvent replacement and hydrophobic modification and consequently leading to the higher cost and environmental pollution due to the large usage of organic solvents and modifiers (Yan et al., 2019). Yan et al. (2019) also mentioned the importance to design greener method of APD in order to achieve good formability of silica aerogels via APD. APD has a key advantage when it is compared to supercritical drying process as it is able to remove pore liquids from wet gels effectively without causing any shrinkage and creation of cracks which commonly due to capillary pressure and the condensation of surface silanol groups (Si-OH) (Hüsing & Schubert, 1998). There are two main approaches to prepare aerogels; first, the monolithic aerogels should be aged in a silane precursor to intensify the mechanical strength of aerogels in order to resist the capillary forces (Davis et al., 1992; Haereid et al., 1994). Secondly, the solvent exchange process should be followed by covering the surface of silanol groups by alkyl groups in order for the gel to experience “spring-back” effect after shrinkage caused by the repulsion between the alkyl groups (Patent No. US 5565142, 1996; Patent No. US 5948482A, 1999).

Freeze-drying process is considered to be the best method for solvent removal and obtain dried product at the highest quality (Ratti, 2012). It is further explained that this method is an outstanding route in order to get dried cellulosic cryogels and sponges with exceptional properties like high porosity, low density and high specific surface area (Zaman et al., 2019). This drying process comprises of three steps which includes freezing, primary drying and secondary drying. The freeze step is the most crucial step in the freeze-drying process and it should avoid having interstices with concentrate liquid to get all the drying is carried out by sublimation (Simón-Herrero et al., 2016). Simón-Herrero et al. (2016) also mentioned that the freezing temperatures range from -50 and -80 °C. Additionally, the freezing rate governs the size of ice crystals and thus the porosity of the dry layer which subsequently affect the drying time (Hammami & René, 1997). It was also mentioned that cellular membranes irreversibility and final product texture are affected by the extreme crystal size (Simón-Herrero et al., 2016).

Primary drying stage depends on the solid solvent sublimation. This step is the longest step of freeze-drying process as water present in the material is sublimated up to 95% and the pressure is decreased to a very low levels whilst the temperature in the shelves is increased to facilitate solvent sublimation (Kremer et al., 2009; Simón-Herrero et al., 2016).

The secondary drying step on the other hand is often carried out to remove unfrozen water molecules since most of the ice has been removed in the primary step. In order to facilitate both removal of residual solvent, the temperature of the shelves is raised to integers higher than those required in the primary drying step (Zhai et al., 2005). The vacuum pressure is also reduced in this step (Patapoff & Overcashier, 2002).

#### **2.4.2 Advantages of Sol Gel**

Sol-gel method has many advantages which makes it a frequent method to synthesize aerogels. According to Kumar et al. (2015), this method to synthesize nanomaterials can improve the adhesion between the substrate and the top coat. Materials can be easily moulded into complex geometry due to the gel state (Kumar et al., 2015). Another advantage of using this method to synthesize aerogels is homogenization can be achieved in a shorter period of time since the mixing involved low viscosity liquids (Mackenzie, 1988). Mackenzie (1988) further explained that since the homogenization can be achieved at molecular level in such a short interval of time, the reactants are most likely to be equally well mixed when the gel is formed. According to Wenzel (1985), this method enables the controllability of the microstructure of the gels. He further explained that this method enables the dry gels to be made with wide range of densities, surface areas and pore sizes.

#### **2.5 Property of Aerogels**

Generally, aerogels are a type of material that possesses numerous outstanding physical characteristics such as low mass densities, continuous porosities and high surface areas. The property of aerogel varies with the types of aerogel. However, the general agreement on the mechanical behavior and property for this literature review will be focusing on silica aerogel.

Aerogels are generally described as brittle materials like glasses and the stress-strain relation evolves like any other elastic material towards fracture (Woignier et al., 2009). Aerogel is a type of material which exhibit a very low density (0.004 – 0.500 g/cc) with an open crossed-linked network having a particle size of less than 10 nm and pore size of less than 50 nm (Aegerter et al., 2011; Mahadik et al., 2016). This material also possesses high porosity of 80 – 99.8%, surface area (500 – 1200  $m^2/g$ ), low thermal conductivity (0.017 – 0.05 W/m K) and hydrophobicity (in terms of the contact angle of water with the aerogel surface  $> 90^\circ$ ) and etc. (Fricke, 1988; Kistler, 1931; Pajonk, 1998; Rao & Kulkarni, 2002). This material also exhibit low water vapor diffusion resistance and good fire ratings which makes it a favourable material for the application of thermal insulation application (Ganobjak et al., 2019). Ganobjak et al. (2019) further inferred that for building thermal insulation, aerogels are able to refurbish small space or where a thick insulation would alter the appearance of the building abruptly. Gonobjak et al. (2019) also demonstrated in their studies that aerogels are prone deterioration with a prolong exposure to temperatures above 70°C and at a high relative humidity of more than 90%.

## **2.6 Biodegradable Aerogels**

Biodegradability has been widely discussed in the recent years. With the emerging of new technologies, there have been numerous researches on the synthesis of aerogels from biodegradable materials. To name a few are cellulose aerogels, alginate-based aerogels, and even aerogels derived from clay and biodegradable polymers.

## **2.7 Cellulose Aerogels**

Cellulose is the most abundant natural polymers on this planet. It possesses distinctive properties from other petroleum-derived polymers like biocompatibility, biodegradability, thermal stability, chemical stability and cost effective (Habibi et al., 2010). In particular, besides its ability to biodegrade, cellulose also possess outstanding mechanical properties such as high porosity, large surface area and low density (Long et al., 2018). Due to these properties, cellulose has become a promising material for future researches. Figure 2.4 summarised the preparation and application of cellulose aerogels.



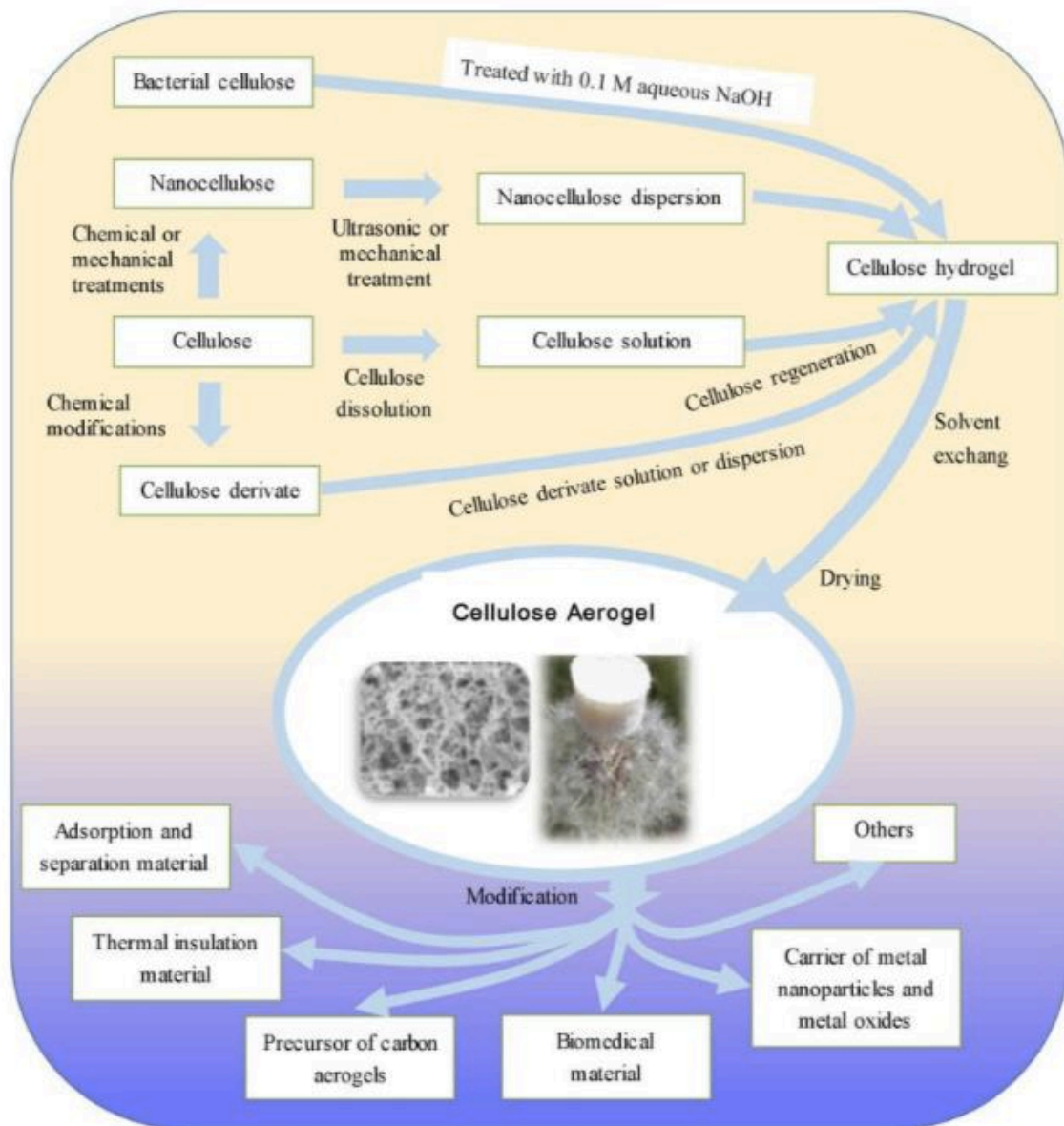


Figure 2.4 Preparation and application of cellulose aerogels (Long et al., 2018)

### 2.7.1 Preparation of Cellulose Aerogels

Generally, according to Long et al. (2018) the preparation of cellulose aerogels includes three steps namely the dispersion of cellulose or cellulose derivatives, sol-gel process and the drying process to obtain aerogels.

1. Dispersing of cellulose or cellulose derivatives

Plants and plant-based materials can be the source to extract cellulose such as rice straw, cotton, wood, cannabis and etc. The properties of cellulose such as its size, degrees of crystallinity, thermal stability and its degree of polymerization varies with its derivative source, extraction processes during production (pre-treatment, post-treatment and disintegration processes (Lee et al., 2015; Trache et al., 2016). Lee et al. (2015) further explained that due to this reason, the morphology of the cellulose is highly depended from the derivative source.

The mechanical property and the moisture affinity of aerogel materials can be enhanced by cellulose and its derivatives (Ahmadi et al., 2016; Nguyen et al., 2016; Seantier et al., 2016). According to Long et al. (2018), by using cellulose as the precursor to synthesize aerogels, there are several advantages that can be achieved which are;

1. Renewable and inexhaustible cellulose derivative reserve
2. Cross linking agents are not required in the synthesis process as cellulose structure is enriched with hydroxyl groups which makes the preparation of the aerogel simpler
3. The improvement of structural characteristics and mechanical properties of cellulose aerogels through chemical modification is easier to accomplish.

## 2. Sol-gel process to form the cellulose aerogels

Sol-gel process is also known as gelation process at which the material transforms from sol liquid state to solid gel state (Long et al., 2018). Long et al., (2018) also mentioned that in order to retrieve solid gel phase, the agglomeration of polymers in cellulose suspension or solution must be done. Alternatively, phase separation process can be used through coagulative regeneration. Regeneration is simply the solvent exchange with non-solvent that will lead to a desolvation of cellulose molecules and reconfiguration of intra and intermolecular hydrogen bonds.

Shen et al. (2016) explained that order to form a 3D interconnected structure which converts the material into a solid gel phase the process should either add

crosslinking agents to the liquid sol or inducing colloidal particle aggregation.

### 3. Drying process of aerogels to retrieve the 3D porous structure

The drying process in the preparation of cellulose aerogels is supercritical carbon dioxide drying. Long et al. (2018) explained that aerogels prepared through a supercritical carbon dioxide drying often exhibit a cauliflower-like arrangement of cellulose. This drying method utilizes the two-way transfer of super critical carbon dioxide and gel solvent via the pores of the wet gel (García-González et al., 2011).

The mechanism of drying through supercritical carbon dioxide drying are divided into several sequence. First, the expansion of the liquid is caused by the high dissolution of supercritical carbon dioxide in the liquid sol gel which consequently causes spillage of excess liquid out of the get network (Long et al., 2018). Secondly, the content of carbon dioxide in the pore gel liquid is directly proportional to time until supercritical state is achieved for the fluid mixture in the pores (Long et al., 2018). Finally, with the presence of the supercritical liquid mixtures in the pores of no liquid phases resulted in the prevention of pore collapse in the gel structure (García-González et al., 2011).

#### **2.7.2 Properties of Cellulose Aerogels**

Cellulose aerogels have a specific surface area of 10 to 975  $m^2/g$ , porosity range from 84.0% to 99.9% and the density ranges from 0.0005 to 0.35  $gcm^{-3}$  (Long et al., 2018). These mechanical properties exhibit by cellulose aerogels are comparable to the traditional and conventional silica aerogels or synthetic aerogels. Long et al. (2018) further explained that cellulose aerogels possess greater value in terms of its compressive strength which ranges from 5.2 kPa to 16.67 MPa.

#### **2.8 Starch Aerogels**

Starch is a promising renewable, biodegradable and low cost for a bio-based aerogel forming material. Among many starch sources, wheat starch is widely chosen to synthesize aerogels. Wheat starch is potential to form the 3D polymeric structures of starch hydrogels

(Maningat et al., 2009). Maningat et al. (2009) further explained that wheat starch composed of 75% amylopectin and 25% amylose. Amylose is a linear polymer of  $\alpha[1 \rightarrow 4]$  linked d-glucose whilst amylopectin is a linear polymer which has a higher molecular weight than amylose and is a branched polymer with  $\alpha[1 \rightarrow 4]$  and  $\alpha[1 \rightarrow 6]$  bonds (Kenar et al., 2014).

### **2.8.1 Properties of Starch Aerogels**

The density of starch aerogels depends on several factors. Ubeyitogullari and Ciftci (2016) mentioned that with the increment of gelatinization temperature, the density of the aerogels decreases at all concentrations. Glenn et al. (2008) inferred that the drop in the density is caused by the high gelatinization temperature which resulted in the formation of more fibrous starch networks. Ubeyitogullari and Ciftci (2016) reported that the lowest densities that they have obtained is at 120°C ( $0.05 \text{ g/cm}^3$ ), 130°C ( $0.04 \text{ g/cm}^3$ ) and 140°C ( $0.03 \text{ g/cm}^3$ ) with no obvious distinction between these densities.

In another finding conducted by García-González and Smirnova (2013), it is reported that the densities for corn and pea starch increases with the increased in starch concentrations from 7 to 15% with the lowest density of  $0.15 \text{ g/cm}^3$  recorded at 7% corn starch. For a microcellular foam derived from wheat starch obtained at 8% concentration corresponds to the density of  $0.23 \text{ g/cm}^3$  (Glenn & Iriving, 1995). Glenn and Iriving (1995) showed that the densities and foams of starch aerogels are strongly correlated with the compressive strength and its elasticity. Therefore, amylose content is significant in determining the mechanical properties of starch aerogels. Several factors that contributed to weak mechanical properties of starch-based aerogels are starch remnants, irregularity of pore sizes and starch granule remnants (Glenn & Iriving, 1995).

The mechanical properties of starch aerogels can be enhanced with the integration of non-starch ingredients (Zhu, 2019). In a study conducted by Ago et al. (2016) proven that the Young's modulus and yield stress in compression mode is significantly increased with the incorporation of cellulose microfibrils through the increment of the cell wall thickness. On the similar note, Zhang et al. (2017) analyzed that the addition of starch in composite melamine-formaldehyde aerogels had improved the mechanical durability and elasticity

when compared to pure malamine-formaldehyde aerogels. Zhang et al. (2017) also inferred that the starch added helped to reduce the relaxation of the polymer chains thus reinforcing the network of hybrid aerogels. In a similar studies conducted by Wang et al. (2018) has proven that the addition of starch into konjac glucomannan based aerogels had improved the elasticity of the resulting aerogels. This is done via the reduction of the pore size and the increment of the evenness of pore distribution (Wang et al., 2018). Wang et al. (2018) also postulated that the improving the mechanical strength of the aerogels might compromise someother mechanical properties of the aerogels such as its thermal conductivity.

### **2.8.2 Morphology of Starch Aerogels**

Every aerogel has three dimensional and open porous structures. According to Ubeyitogullari and Ciftci (2016), as the starch concentration increases, the density of the structure increases because the sizes of the network openings decreases. This inference also corresponds the the density of the starch aerogels with the increased starch concentration. The structures of the starch aerogels obtained by Ubeyitogullari and Ciftci (2016) mostly composed of interconnected fibrils and nanopores. Similar nanoporous structures were also reported for corn and pea starch aerogels as reported by García-González and Smirnova (2013). Zhu (2019) mentioned that the crystallinity of the native starch can be disrupted by the gelatinization of the aerogels. This disruption in crystallinity resulted in the lost of typical patterns of native starch as analyzed by wide angle X-ray diffraction (Zhu, 2019).

The microstructures of starch aerogels differ in different studies and this may be contrubuted by certain factors such as starch concentration, pressure and temperature during processing, gelatinization and retrogradation conditions and the rate of supercritical carbon dioxide drying (García-González & Smirnova, 2013; Kenar et al., 2014; Ubeyitogullari & Ciftci, 2016). Starch concentration in starch aerogels has a significant impact in its microstructures. Unstable hydrogels resulted from low starch concentrations and too high starch concentration caused a major decrease in the processability of the starch system due to its high viscosity (García-González & Smirnova, 2013). Druel et al. (2017) mentioned that specific surface area of the aerogels can be increased with the increment of the amylose content. On the other hand, increasing the retroradation time led to a reduction of specific surface area (Zhu, 2019). This phenomenon is due to the heterogenous structure

which was unable to stand the pressure from the drying process resulted from the high retrogradation of amylose. Generally, aerogels which are derived from starches with lower amylose content often resulted in lower specific surface area and a higher density (Zhu, 2019). Druel et al. (2017) indicated that the type of starch and a suitable ratio of amylose/amylopectin are significant in determining the microstructures of aerogels.

In certain conditions of the process, aerogels exhibit higher surface area caused by the high shearing rate during starch gelatinization due to a more even distribution of starch and less granular remnants (Zhu, 2019). On the other hand, the decrease surface area of aerogels is caused by an increasing carbon dioxide flow rate during the supercritical drying of aerogels (Zhu, 2019). This phenomenon can be inferred to a higher dissolution of carbon dioxide and a more expanded lipid phase inside the pores of the aerogels (García-González et al., 2012).

Cross-linking which is one of starch modifications has the potential to change the microstructure of the starch aerogels (Abhari et al, 2017). The uniformness of the pore distribution of the aerogels can be attributed by the cross-linking of starch (Zhu, 2019). Zhu (2019) further postulated that the cross-linking of starch may contribute to the stability of the starch hydrogels and aerogels through the strengthening of the starch network.

In a case dependent manner, the microstructures of starch aerogels can be also affected significantly by the addition of non starch ingredients ingredient for the preparation of composite starch aerogels (Zhu, 2019). The pore size of starch-glucomannan-wheat straw powder decreased with the addition of wheat straw powder due to the interruption of starch network during retrogradation (Y. Wang et al., 2018).

### **2.8.3 Thermal Properties of Starch Aerogels**

Starch based aerogel's major application was as thermal insulating material (G. M. Glenn & Iriving, 1995; Y. Wang et al., 2018). Glenn and Iriving (1995) showed that there was a similarity between starch aerogels and the commercial insulation samples in terms of thermal conductivity. Starch aerogels exhibit a low thermal conductivity (Koebel et al., 2012). Koebel et al. (2012) inferred that the low thermal conductivity of starch aerogel is

contributed by the very small pore size which is less than the mean free path of air molecules and its densities.

In another studies conducted by Druel et al. (2017) proved that the thermal conductivity of starch aerogels depended on the types of starch used and its processing conditions. Zhu (2019) mentioned that aerogels that were derived from pea starch has the lowest thermal conductivity of less than air when it was compared with other starch based aerogels derived from waxy and regular potato and high amylose maize. This results concluded that the low thermal conductivity in starch aerogels were contributed by only special combination of amylose and amylopectin (Zhu, 2019). Another contributing factor that affect this property is the retrogradation time (Druel et al., 2017). Increasing the retrogradation time resulted to the increase thermal conductivity via the reduction of the specific surface area (Druel et al., 2017).

In a study conducted by Ubeyitogullari and Ciftci (2016) showed that there was a similarity between wheat starch and its aerogels in terms of thermal stability. Thermal degradation occurred rapidly at 280-330°C (Zhu, 2019). Ubeyitogullari and Ciftci (2016) mentioned that the formation of ash and char was much faster in starch aerogel than its native form. Zhu (2019) postulated that this occurrence may have occurred due to its more open structure which allowed more efficient heat penetration.

#### 2.8.4 Production of Starch Aerogels

Production and properties of starch-based aerogels based on previous researches and studies are shown in Table 2.1.

Table 2.1 Past researches on the production of starch aerogels

<b>Starch Type</b>	<b>Fabrication Method</b>	<b>Major Findings</b>	<b>References</b>
<b>Maize Starch</b>	The starch was turned into gel and passed through ethanol solvent exchange and supercritical carbon	The network and mechanical stability of the starch aerogels is significantly reduced with the increment of drying time. Appropriate	García-González et al. (2012)

	dioxide exchange drying process	supercritical carbon dioxide corresponded to the highest surface area	
<b>High amylose maize starch (70% amylose)</b>	Starch-sodium palmitate complexes derived hydrogels undergone ethanol solvent exchange prior drying with supercritical carbon dioxide drying	The aerogels obtained from the manipulation of depressurization of supercritical carbon dioxide drying exhibited densities of 0.120 – 0.185 $g/cm^3$ and Brunauer-Emmet-Teller (BET) specific surface area. The volume and the surface areas had no correlation with the depressurization of supercritical carbon dioxide drying.	Kenar et al. (2014)
<b>Maize Starch</b>	Trisodium citrate was used to cross-link the starch in suspension. The modified starch was gelled and freeze-dried	The hardness and the crystallinity of the starch aerogels can be increased through cross-linking. The uniformity of pore distribution can also be enhanced by cross linking process	Abhari et al. (2017)
<b>Wheat Starch</b>	Prior to retrogradation, the starch suspension was gelatinized at 130°C in the presence/absence of sodium metaphosphate	Aerogels with an average pore size of 18nm, density of 0.11 $g/cm^3$ and surface area of 61 $m^2/g$ was obtained. The resistant starch (RS)	Ubeyitogullari et al. (2018)



	(STMP) in a high-pressure reactor. The starch hydrogel was then subjected to solvent exchange and supercritical carbon dioxide drying	content of the aerogel was significantly increased due to the cross-linking. The RS content in the aerogels produced without STMP was largely resistant to cooking caused by retrogradation	
<b>Regular and waxy potato, high amylose maize starch and pea starches, pure amylose</b>	The starch was turned into gel and passed through ethanol solvent exchange and supercritical carbon dioxide exchange drying process	Pea starch aerogels exhibited the lowest thermal conductivity (0.021-0.023 W/mK). However, pea starch aerogels had the highest density and surface area compared to other starch aerogels. The resistance to volume shrinkage and the specific surface area can be increased with the increment of amylose content. On the other hand, increasing the retrogradation time will reduce the specific surface area while increasing the thermal conductivity and enhancing the mechanical properties.	Druel et al. (2017)
<b>Starch (high amylose maize) based carbon aerogels</b>	The starch is mixed with Graphite up to 20% before milling gelatinization,	The addition of graphite triggered the development of strong interaction between graphite and	García et al. (2018)

	retrogradation, solvent exchange, freeze drying and pyrolyzed at 800°C under vacuum	starch matrix. This process decreased the number of graphite layers by more than 50% and particles size up to 24 nm	
<b>Starch based carbon aerogels (potato, rice, maize) based carbon aerogels</b>	The gelatinized and retrograded starch was subjected to ethanol exchange prior to drying at 50°C. The aerogels were then pyrolyzed at up to 900°C for six hours.	The maize starch carbon aerogels had the highest surface areas at 800°C. Rice starch carbon aerogels had the highest surface areas at temperatures above 800°C. Among all the	Bakierska et al. (2017)
<b>Melamine, soluble starch formaldehyde</b>	The blend of formaldehyde, soluble starch and melamine was subjected to heating, solvent exchange and supercritical carbon dioxide drying	There was an insignificant volume shrinkage from gel to aerogel. The retrieved aerogels exhibited a pore diameter of 13 nm and specific surface area of 370 $m^2/g$ . The aerogels also exhibit high mechanical durability and elasticity	Zhang et al. (2017)
<b>Potato starch, konjac glucomannan, wheat straw powder and gelatin</b>	Prior to freeze drying, starch glucomannan wheat straw gelatin was in water to form aerogels	The composite aerogels had the thermal conductivities ranging from 0.046 to 0.053 W/mK. The aerogels with the lowest thermal conductivity exhibit a density of 0.043 $g/cm^3$ and porosity of 94.5%. the addition of the starch to	Wang et al. (2018)

---

the composite aerogels enhanced the mechanical strength whilst the incorporation of wheat straw reduced the pore size.

---

### 2.8.5 Various Application of Starch Aerogels

The various application of starch aerogels based on previous studies and researches is shown in Table 2.2.

Table 2.2 Various application of starch aerogels

Uses	Type of Aerogels	Major Findings	References
<b>Encapsulation and delivery of bioactive compounds/drugs</b>	Starch aerogels loaded with ketoprofen	11% (w/w) of the aerogels is reached for its loading capacity of ketoprofen. In vitro release test has proven that the release of ketoprofen was more sustained than the pure sample	García-González and Smirnova (2013)
<b>Encapsulation and delivery of bioactive compounds/drugs</b>	Maize starch aerogels with the addition of benzoic acid and ketoprofen	The amorphous drug was injected into the aerogels. The loading amount of ketoprofen and benzoic acid in the starch aerogels reached up to $1.0 \times 10^{-3}$ and $1.7 \times 10^{-3} \text{ g/m}^2$ . The drug released from the starch aerogels were followed by dissolution as shown from the in vitro test	García-González et al. (2015)

---

<b>Encapsulation and delivery of bioactive compounds/drugs</b>	Maize starch aerogels which contained five different drugs with low water solubility for oral delivery	The addition of the drugs into the aerogels significantly increased the bioavailability and the dissolution as shown in vitro and in vivo (Winstar rats) studies	Lovskaya et al. (2015)
<b>Tissue engineering</b>	Starch/ $\kappa$ -carrageenan composite aerogels	In order to make homogenous nanostructured and mechanically stable PEDOT (poly (3,4-ethylenedioxythiophene) which was compatible with the SH-SY5Y human neuroblastoma cells, aerogels were used as templates. The mechanical and electrical properties of the PEDOT materials were improved significantly by the aerogels	Zamora-Sequeira et al. (2018)
<b>Thermal insulating material</b>	Aerogels derived from waxy and regular potato, high amylose maize and pea starches	By comparison, aerogels derived from pea starch had the lowest thermal conductivity. The thermal conductivity was attributed by both amylose and amylopectin	Druel et al. (2017)
<b>Carbon dioxide adsorption</b>	Wheat starch aerogels	The aerogel was able to adsorb isosteric heat of -32.1 kJ/mol. The aerogel has potential in the application	Anas et al. (2017)

## **2.9 Executive Summary**

Based on the literature review conducted, until now there has been little work in specifying or detailing the application of ambient pressure drying in the synthesis of starch-based aerogels. In its underline reason, it is believed that the common methods of drying which are supercritical carbon dioxide drying and freeze drying consume less time by having the advantage of skipping the chemical modification of the sample and getting the desired morphology of the aerogels in short period of time. Hence, the application of ambient pressure drying in synthesizing starch-based aerogel need to be explored in detail and are discussed in the following section of the paper.

# CHAPTER 3

## METHODOLOGY

### 3.1 Introduction

This chapter outlined the overview of the methodology of the overall research. The research includes synthesizing aerogels from various sources of starch and the methods to synthesize them. The summary of the process to synthesize starch aerogels are presented in the flowcharts. This chapter also housed the flowcharts that depicted the processes involved in synthesizing the starch aerogels. The flowchart in Figure 3.2 presented the overall proposed process to synthesize starch aerogels. In addition, this chapter also includes the characterization of samples which includes Scanning Electron Microscopy (SEM), density measurement and thermal conductivity test.

### 3.2 Materials

Commercial wheat starch used were purchased from local grocery store in Kuching Sarawak, Malaysia. Isopropanol is used obtained. Acetone is used as obtained. Trimethylchlorosilane (TMCS) is used as obtained.

### 3.3 Synthesis of Starch Aerogels

The formation of aerogels starts with gel formation from aqueous solution at which the starch solution was converted into hydrogel by gelatinization. The step is followed by solvent exchange or replacement of water filling the pores of the gel structure by isopropanol which resulted in alcogel. Finally, the ethanol contained in the gel is removed from the gel through supercritical carbon dioxide drying. The processing steps for the synthesis of aerogels is depicted in Figure 3.1.

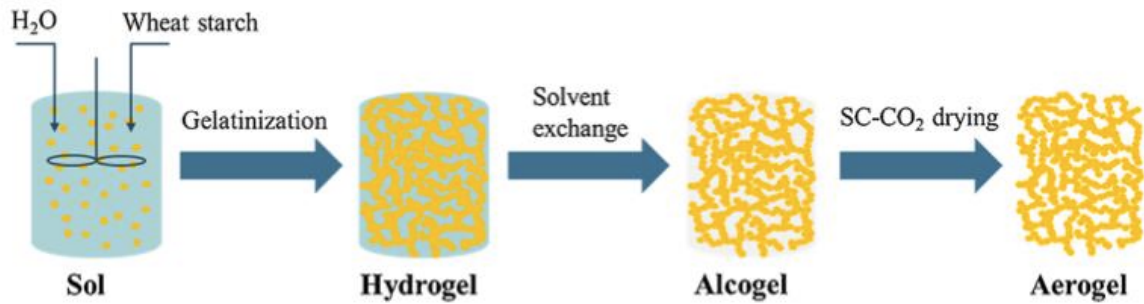


Figure 3.1 Schematic diagram of processing steps to synthesize starch aerogels (Ubeyitogullari & Ciftci, 2016)

### 3.3.1 Hydrogel Formation

The formation of hydrogel monoliths was in accordance to the method proposed by García-González and Smirnova (2013) with some modifications. The starch powder was mixed into distilled water to obtain various concentrations. Trimethylchlorosilane (150 mg) is added dropwise into the starch suspension. The starch dispersions at 5%, 10% and 15% w/w were then stirred to trigger gelatinization process until viscous gels were obtained. The dispersions were stirred at predetermined temperatures set for gelatinization 100°C. This temperature is chosen based on predetermined set of temperatures for gelatinization (100, 120, 130 and 140°C) wheat starch aerogels as proposed by Ubeyitogullari and Ciftci (2016). The viscous gel was poured into cylindrical polypropylene molds of specific dimensions (1.5 cm diameter and 10 cm length). Polypropylene molds have less irregularities compared to other molds e.g. glass molds (Ulker & Erkey, 2014). Due to this reason, polypropylene molds were chosen. To prevent loss of water, the samples were sealed with parafilm and placed in the fridge for 48 hours for retrogradation.

### 3.3.2 Solvent Exchange and Esterification

The hydrogels were removed from the polypropylene molds after 48 hours of retrogradation. The hydrogels were then cut into 2 cm length monoliths. The alcogels were then formed through solvent exchange process. In this process, water in the monolith was replaced with ethanol using a one-step solvent exchange procedure. In this procedure, the hydrogel monoliths were soaked in 100% (v/v) of isopropanol with 24-hour residence time. The esterification process was adopted from a study conducted by Sehaqui et al., (2014)

with some modifications. This esterification process is part of surface modification process for the alcogel monoliths.

### **3.3.3 Ambient Pressure Drying**

The drying process was adopted from a study conducted by Sehaqui et al. (2014) with some modifications. To conduct the drying process, the monoliths was removed from the reactive solution and introduced in an oven at 65°C for two hours or until constant weight is achieved. Oven was used in this step to facilitate and speed up the drying process.



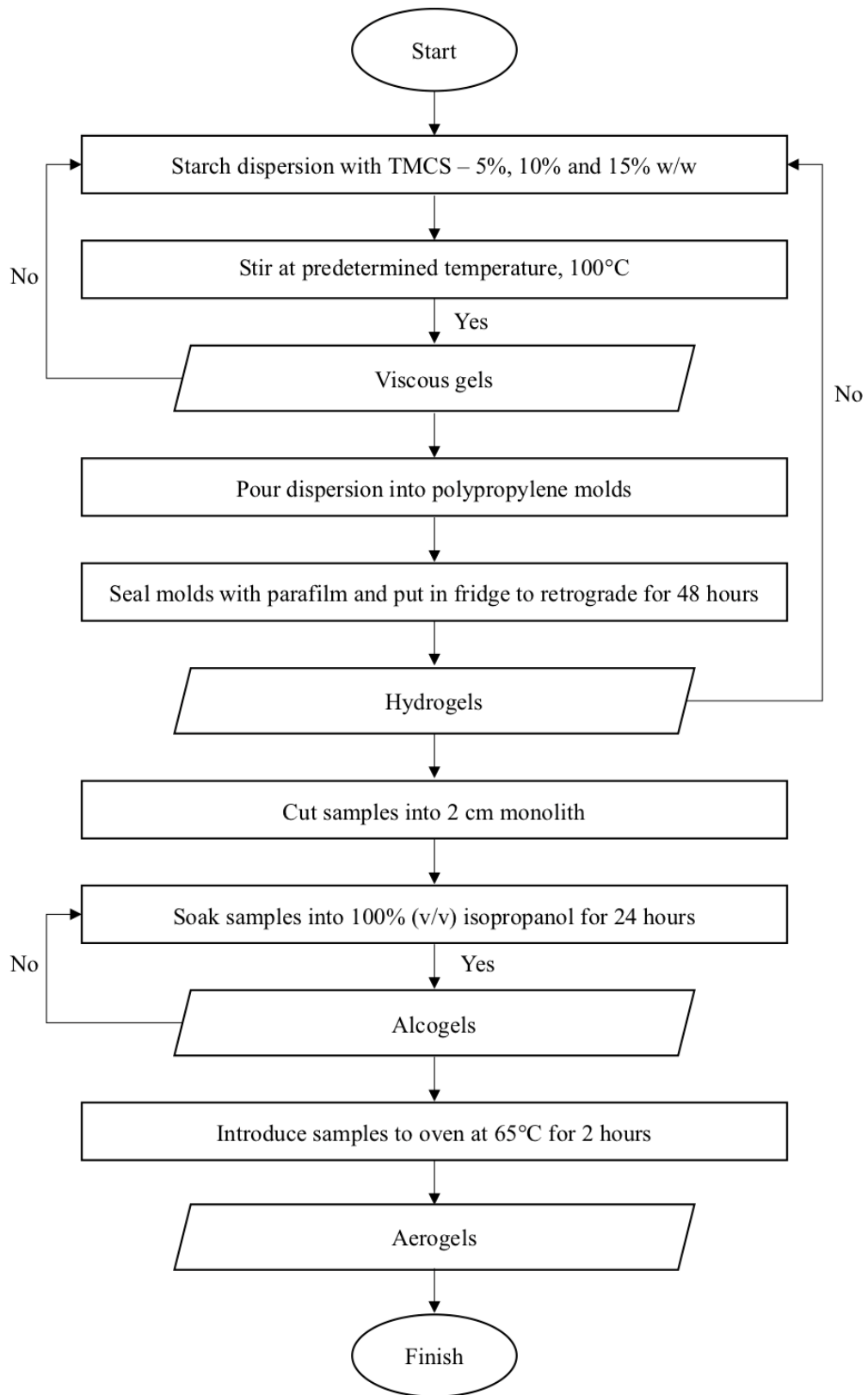


Figure 3.2 Flowchart for the formation of wheat starch-based aerogel

### 3.4 Sample Characterization

#### 3.4.1 Scanning Electron Microscopy

The morphology of the samples was observed using a scanning electron microscope (SEM) (Hitachi TM3030). The samples are pre-coated with a thin and fine tungsten layer by an ion sputtering device which able to overcome the inherent charging effect. The specification of the SEM is shown in Table 3.1.

Table 3.1 TM3030 specification

Items	Description
Magnification	15 to 30, 000x (digital zoom: 2x, 4x)
Observation Condition	5kV/15kV/EDX
Observation Mode	Standard mode Charge-up reduction mode
Image Mode	COMPO/Shadow 1/Shadow 2/TOPO
Sample Stage Traverse	X: ±17.5 mm, Y: ±17.5 mm
Maximum Sample Size	70mm in diameter
Maximum Sample Height	50mm

#### 3.4.2 Density Measurement

The completed sample aerogel is removed from the PLA mould and its dimensions are measured by using a digital Vernier calliper. This is to calculate the volume of the aerogel. The hydrogel is the weighed on a digital weighing scale and the density is calculated by using Equation (3.5).

Density;

$$\rho = m / V \quad (3.5)$$

Where;

$\rho$  : Density of the sample (kg/m<sup>3</sup>)

$m$  : Mass of the sample (kg)

$V$  : Volume of sample (m<sup>3</sup>)

### 3.4.3 Thermal Conductivity Test

The type of thermophysical properties that needed to be measured is thermal conductivity. It is measured by using the heat flow method in accordance with the ASTM E1225-99 Standard test method for thermal conductivity of solids by means of the guarded comparative longitudinal heat flow technique as seen in Figure 3.3 and Figure 3.4.

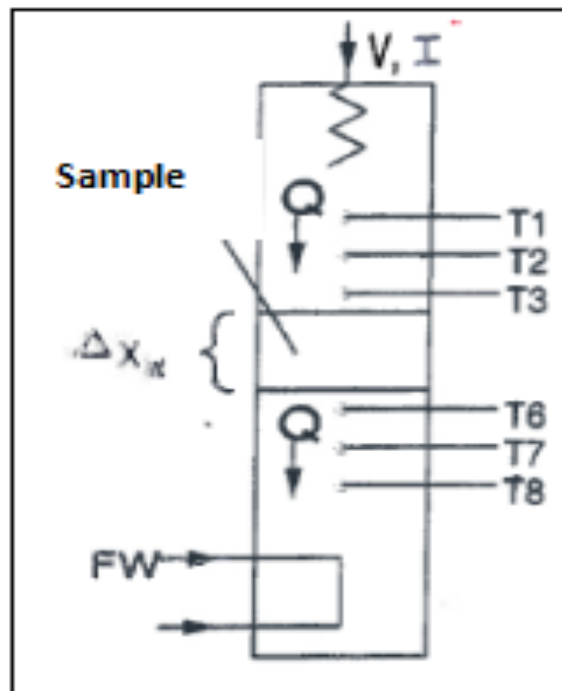


Figure 3.3 Experimental set up outline (PA Hilton H112A Manual)

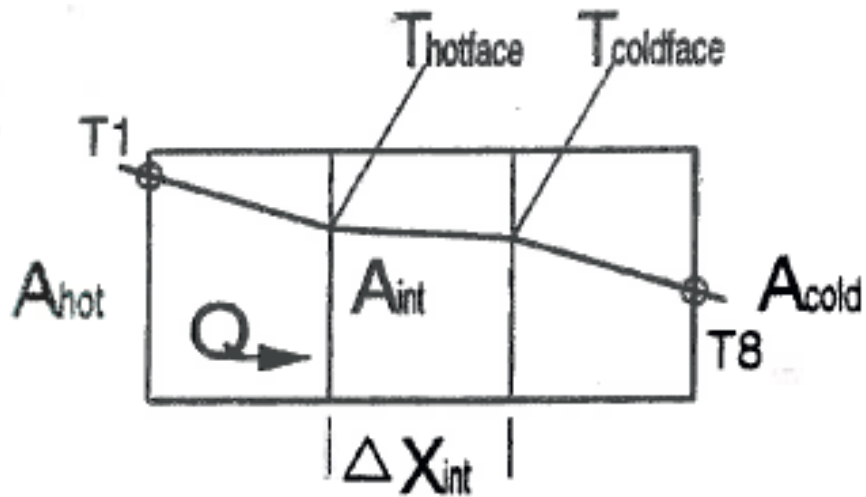


Figure 3.4 Temperature measurement outline (PA Hilton H112A Manual)

The solidified hydrogel sample in the holder is inserted into the testing region of the heat conduction unit as can be seen in Figure 3.5.

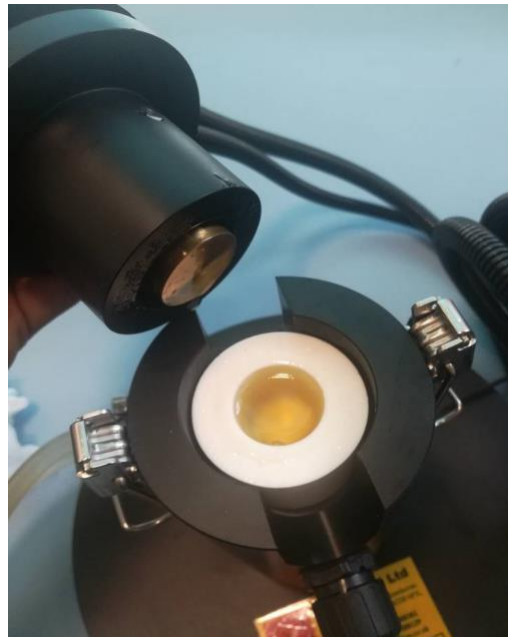


Figure 3.5 The position of the hydrogel sample inside the heat conduction unit

The instrument used is PA Hilton H112A Linear Heat Conduction Unit which can be found in the Basic Thermodynamics Lab. First, the hydrogel specimen and the holder is place in the two brass terminal of the conduction unit. Constant heat flux of ranging from 1W-2.5W. is supplied from the hot terminal of the machine. Meanwhile, at the cold terminal, cooling process is done by circulating water at a constant rate of 4L min<sup>-1</sup>. Six

thermocouples, three at each terminal; (T<sub>1</sub>, T<sub>2</sub> and T<sub>3</sub>) at the hot terminal and (T<sub>6</sub>, T<sub>7</sub>, T<sub>8</sub>) at the cold terminal as can be seen in Figure 3.6 are used to measure the temperature every 2 minutes up to 20 minutes. The temperature will keep on increasing until it reaches the steady-state condition at which the temperature change is at a tolerance level of  $\pm 1^\circ\text{C min}^{-1}$ . The interface temperature of the hot (T<sub>h</sub>) and cold (T<sub>c</sub>) ends of the specimen are calculated by extrapolating the values of all the thermocouples (T<sub>1</sub>-T<sub>8</sub>). The effective thermal conductivity of the hydrogel sample (WmK<sup>-1</sup>), K<sub>c</sub> can be calculated by using these formula;

Heat flow in the hot zone:

$$T_{hot} = T_3 - \left[ \frac{T_2 - T_3}{2} \right] \quad (3.1)$$

Heat flow in cold zone:

$$T_{cold} = T_6 - \left[ \frac{T_6 - T_7}{2} \right] \quad (3.2)$$

The interval temperature (temperature between the hot and cold region) can be calculated by using in Equation 3.3.

Internal temperature, T<sub>int</sub>:

$$T_{int} = T_{hot} - T_{cold} \quad (3.3)$$

Therefore, the thermal conductivity can be calculated as follows:

$$K_C = \frac{\dot{Q} \Delta x_{int}}{A \cdot \Delta T_{int}} \quad (3.4)$$

Where;

T<sub>1</sub> - T<sub>6</sub> : Thermocouple reading

x<sub>int</sub> : Length hot region form cold region, (30mm)

$T_{hot}$  : Heat flow in the hot zone  
 $T_{cold}$  : Heat flow in the cold zone  
 $T_{int}$  : Internal temperature (space between  $T_3$  &  $T_6$ )  
 $A$  : Sample area  
 $K_c$  : Thermal conductivity of sample

# CHAPTER 4

## EXPECTED RESULT AND DISCUSSION

### 4.1 Introduction

This section of the paper reviews the expected results and discussion which corresponds from the proposed method of the experiment. In order to make the comparison consistent despite having limited studies on starch aerogels synthesized via ambient pressure drying, the expected results obtained are solely forecasted based on the collective result of previous studies of similar and specific scope (i.e. other types of starch-based aerogels, polysaccharide-based aerogels, cellulose aerogels). This section discusses on the microstructure of starch-based aerogels, crystallinity of starch-based aerogels, thermal properties of starch-based aerogels, mechanical properties of starch-based aerogels and the factors that affect these parameters.

### 4.2 Structural, physicochemical and functional properties of wheat starch-based aerogels

#### 4.2.1 Effect of drying technique: Ambient pressure drying

One of the fundamental factors that contributed to the microstructure of aerogels is the drying process of the aerogels. Aerogels are typically produced via supercritical carbon dioxide drying, freeze drying and ambient pressure drying. Methods like supercritical carbon dioxide drying and freeze drying are capable of fabricating aerogels while preserving the porosity (El-Naggar et al., 2020). On the opposite of the spectrum, ambient pressure drying is able to fabricate aerogel and compromise most of the porosity of the material as reported by El-Naggar et al. (2020). According to Ubeyitogullari and Ciftci (2016), high shrinkage rate often resulted from air drying due to high surface tension and capillary pressure gradient in the pores as shown in Figure 4.1. The SEM images display that the structure of xerogel is nonporous. However, it is best not to conclude that the

structure of aerogel synthesized from ambient pressure drying will totally be nonporous but instead it is safe to assume that the structure will exhibit a higher porosity than xerogel as the microstructure is attributed to a range of factors. The attributing factors include the type of starch, starch concentration, gelatinization and retrogradation conditions, pressure, temperature and carbon dioxide flow and depressurization rates of supercritical carbon dioxide drying (García-González et al., 2012; Kenar et al., 2014; Ubeyitogullari & Ciftci, 2016).

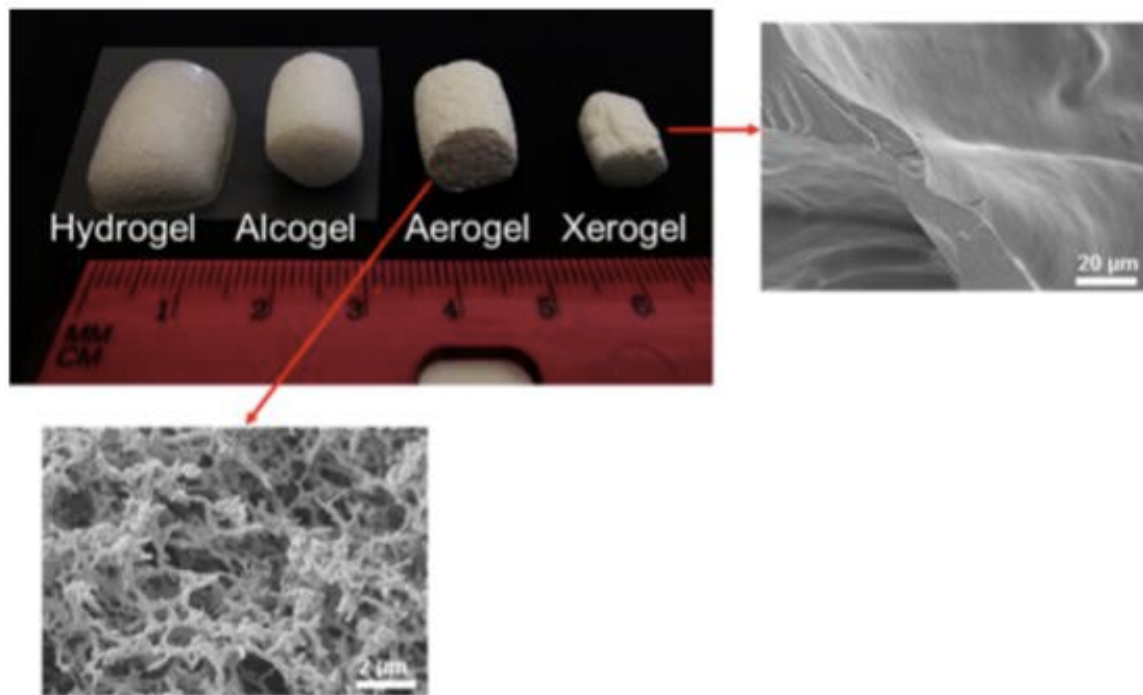


Figure 4.1 Pictures of hydrogel, alcogel, aerogel and xerogel derived from wheat starch (Ubeyitogullari & Ciftci, 2016)

In order to understand the effect of the drying process, it is essential to investigate the possible stresses on the pore walls of the porous materials. As shown in Figure 4.2, it is worthy to note that the pores are assumed to be evenly distributed. As represented by  $F_1$ ,  $F_2$ ,  $F_3$  and  $F_4$  as the capillary pressure is often the outcome from the evaporation of solvent at the gas-liquid interface will transmit to the pore walls.  $F_1'$ ,  $F_2'$ ,  $F_3'$  and  $F_4'$  on the other hand represent the resultant forces on the pore walls in the horizontal direction caused by the capillary pressure. This will result in the imbalance of the forces in the walls. The imbalance will ultimately result in the collapse of the porous structure (Wang et al., 2005).



To overcome the imbalance of the force, there are several modifications that can be adopted which includes (i) decrease the surface tension of the solvent; (ii) improve the mechanical properties of the pore walls; (iii) produce pores with consistent sizes to balance the stress force on the wall; (iv) decrease the angle between the pore and the solvent by enlarging the por size (Aravind et al., 2010).

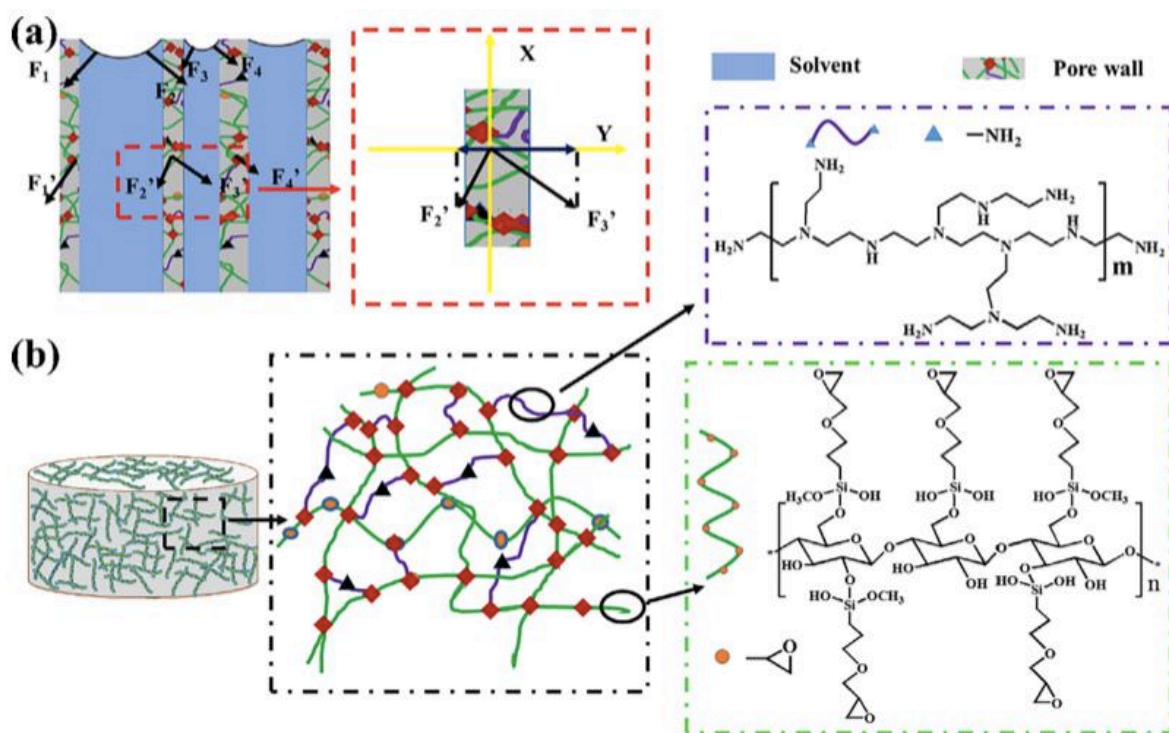


Figure 4.2 The stress analysis of pore walls of porous materials during the drying process and (b) schematics of the cross-linked networks (Li et al., 2019).

Taking into account the attributing factors that affect the microstructure of the aerogels, the starch aerogels' microstructure is more likely to resemble the chitosan-urea aerogels synthesized from a study conducted by Guerrero-Alburquerque et al. (2020). Based on Figure 4.2, the material presents local density variations between regions with predominantly mesopores domains separated by macropores. According to Guerrero-Alburquerque et al. (2020), diameter of 150 and 650 nm are the largest observed pores sizes for supercritical carbon dioxide drying (refer Figure 4.3a, 4.3c) and ambient pressure drying (refer Figure 4.3b, 4.3d) dried aerogels, respectively. Guerrero-Alburquerque et al. (2020) also reported that the APD samples exhibit higher macroporosity is related to

platelet-like structures that most likely were formed by partial structural collapse during evaporative drying (refer Figure 4.3b, 4.3d).

Based on the SEM images in Figure 4.3, both aerogels synthesized via supercritical carbon dioxide drying and ambient pressure drying display a linked particles of ~50 nm in diameter which ranges from 20 to 90 nm (Guerrero-Alburquerque et al., 2020). These figures correspond to a significant mesoporosity within the material. According to IUPAC nomenclature, mesoporous material consists of pores with diameters between 2 to 50 nm.

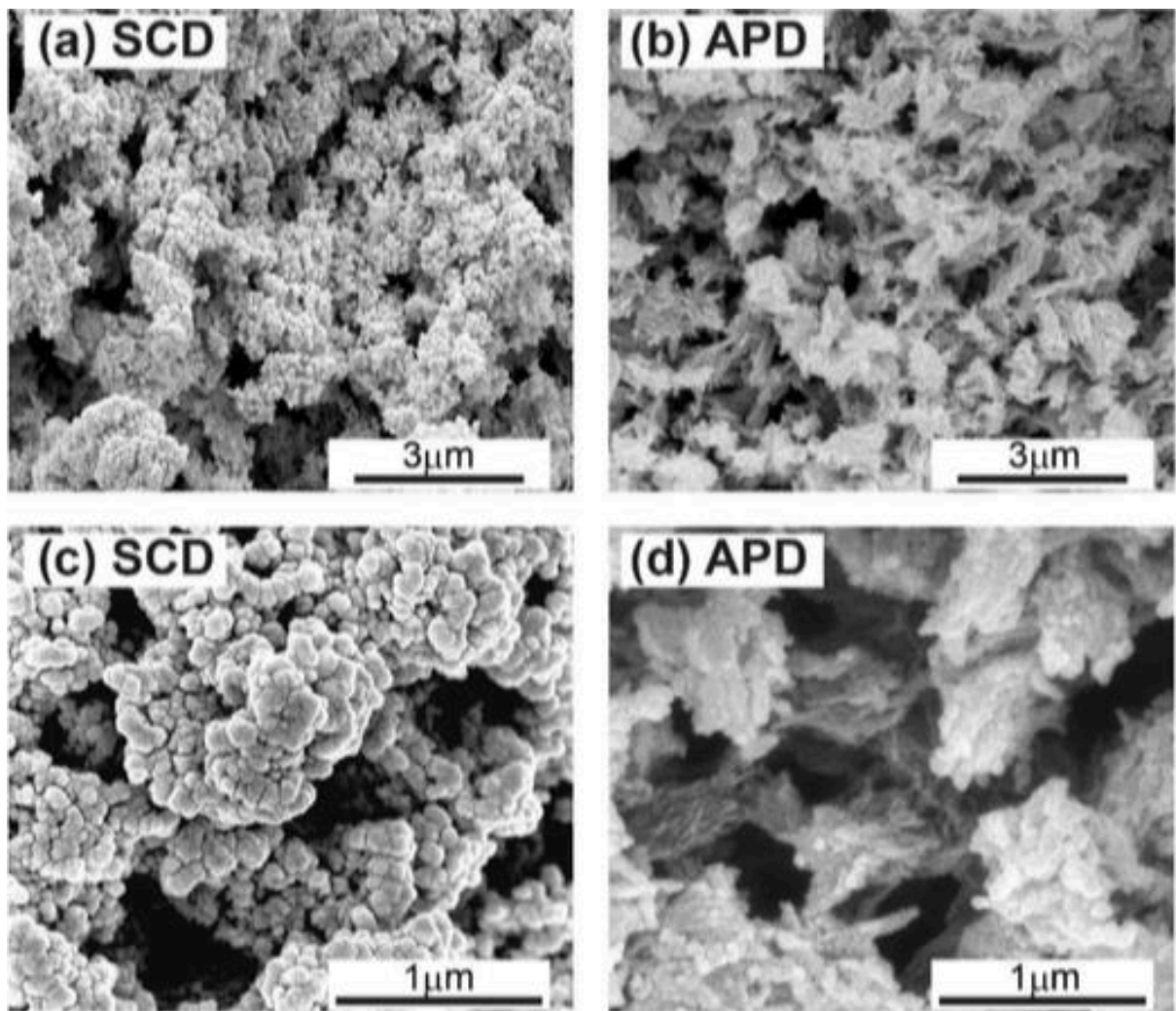


Figure 4.3 SEM images of chitosan-urea gels (a) SCD aerogel (30 000x) (b) APD aerogel (30 000x) (c) SCD aerogel (100 000x) (d) APD aerogel (100 000x) SCD and APD images are from gels prepared from a 5% m/v and 10% m/v chitosan solution, respectively (Guerrero-Alburquerque et al., 2020)

To confirm the nature of mesoporosity of the material, Guerrero-Alburquerque et al. (2020) conducted nitrogen sorption analysis. This analysis confirms the presence of substantial mesoporosity and surface area of the sample. Based on Figure 4.4a, there is a significant nitrogen adsorption in the capillary condensation regime, coalesced with a narrow desorption hysteresis loop corresponds to the sample's mesoporosity for both aerogels dried via supercritical carbon dioxide drying and ambient pressure drying. Significant mesoporosity of the material can also be observed via Barret-Joyner-Halenda (BJH) analysis model for pore size distribution (refer Figure 4.4b).

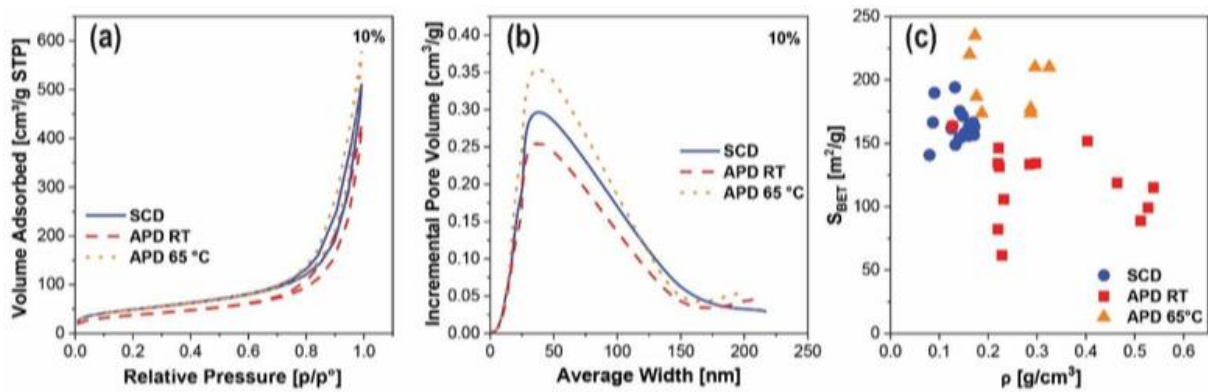


Figure 4.4 Nitrogen sorption data (a) Nitrogen sorption isotherms of 10% chitosan sample (b) BJH desorption plots of 10% chitosan sample (c) Surface area as a function of density for all different chitosan concentrations (Guerrero-Alburquerque et al., 2020).

In another study conducted by Ganesan et al. (2016) suggested that another factors that attributed to the microstructure of the aerogels is the liquid-vapor interface. The liquid-vapor interface and the physical properties of the solvent medium influenced the properties of ambient dried aerogels because the drying takes place by evaporation of solvent molecules (Ganesan et al., 2016). Based on Figure 4.5a and 4.5c (images of lower magnification), both images displayed wrinkling effect due to massive volume shrinkage in the ambient drying conditions. Ganesan et al. (2016) reported that the macropore size ranging between 50 and 120  $\mu\text{m}$ . It is also reported that two pores are connected by a neck point of size ranging between 10 to 50  $\mu\text{m}$ .

The distribution of cellulose fibrils and the details of pore sizes in the cell walls are revealed by the analysis of nanostructure of the material. Referring to Figure 4.5b, the microstructure displayed an agglomerated nanofibrils due to volume shrinkage. Regardless,

the pores in between the nanofibrils are observed. On the opposite of the spectrum (refer to Figure 4.5d), the microstructure presented more agglomeration of the nanofibrils and the pores can hardly be identified between individual fibers. In the same study, Ganesan et al. (2016) also reported that the total porosity or the percentage of pore volume for cellulose scaffolds obtained from isopropanol and ethanol are about 80% and 70% respectively. It is also stated that the BET specific surface area for cellulose scaffolds obtained from isopropanol is 100 m<sup>2</sup>/g (Ganesan et al., 2016). This inferred to the existence of nanofibrils and continuous porous network in the sample. On the other hand, BET specific surface area for cellulose scaffolds obtained from ethanol is about 0.8 m<sup>2</sup>/g (Ganesan et al., 2016). This indicates that the samples exhibit the limitation to find the porous network between the agglomerated fibers.

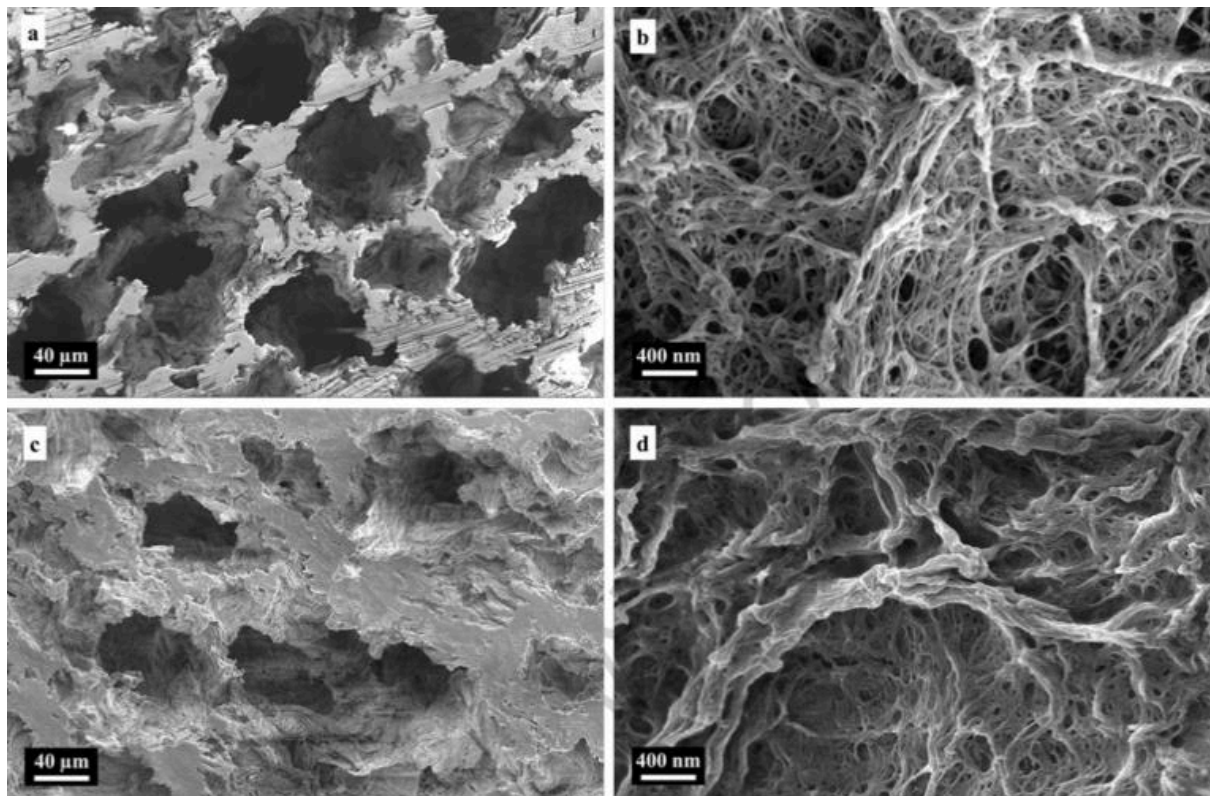


Figure 4.5 The SEM images of cross-sectioned xerogels of cellulose scaffolds obtained from the solvent medium; isopropanol (a and b) and ethanol (c and d) (Ganesan et al., 2016)

The microstructure of aerogels can also be linked with the incorporation of non-starch ingredient or material. As reported by Markevicius et al. (2017) in the study of insulating monolithic silica-based aerogels with short cellulosic fibers, the specific surface area of

aerogels is influenced by the fiber addition regardless of the drying mode. Figure 6 shows the specific surface areas as measured by BET method. According to Markevicius et al. (2017), for both types of composite aerogels, the values are similar. The specific surface area is the largest in the absence of the fibers which counts around 730 m<sup>2</sup>/g, which is in quantitative agreement with other type of silica aerogels of previous studies (Zhao et al., 2015). As expected, with the increase of fiber concentration in the composite, the surface area is observed to show a decreasing trend as shown in Figure 4.6 (refer to dashed line).

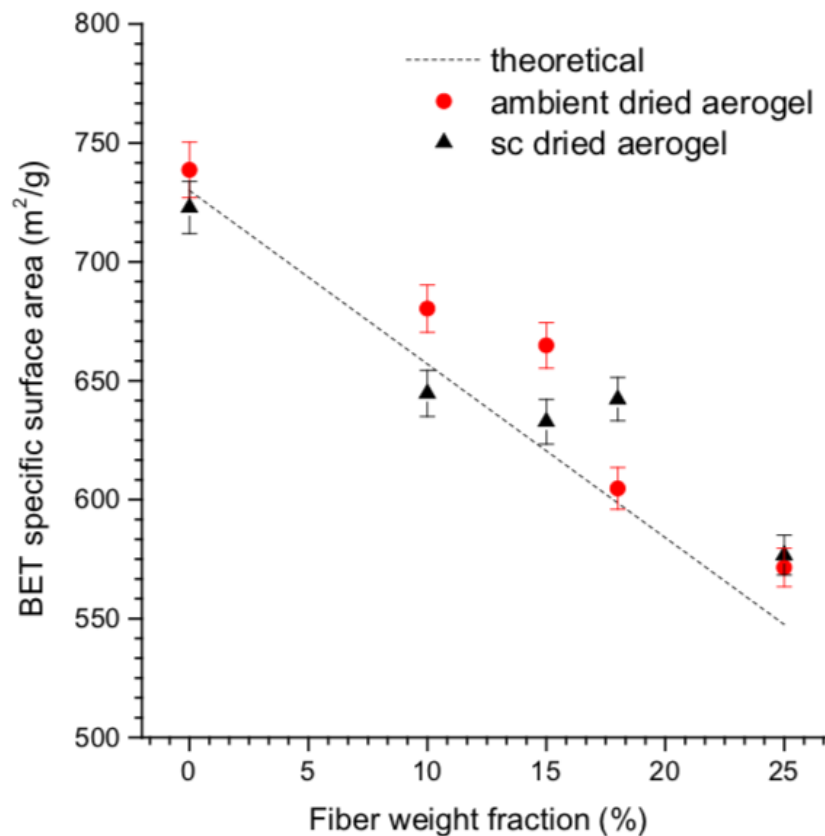


Figure 4.6 BET specific surface areas of the aerogel composites. Dashed line corresponds to the theoretical specific surface area (details in text) (Markevicius et al., 2017)

As reported by Markevicius et al. (2017), the calculation of the theoretical specific surface area was based on a simple “mixing rule” based on the specific surface area of pure silica aerogels. It can also safe to assume that the contribution of fiber to this parameter is zero since the cellulosic fibers specific surface area is negligibly low in comparison to that of silica matrix (Markevicius et al., 2017). Based on Figure 4.6, the presence of fibre does not significantly affect the surface area of the silica matrix itself as demonstrated through the

small experimental deviation from linearity. Based in Figure 6, the specific surface area of the composite still remain high despite high concentration of fibre in the composite i.e. at 25 wt%, the BET specific surface area remains high, higher than 570 m<sup>2</sup>/g.

As shown in Figure 4.7, the high-magnification SEM presents silica phase alone for supercritical dried composite aerogel and ambient pressure dried composite aerogels. During these two drying processes, it can be observed that the highly porous structure of the silica is still preserved and remains in the mesopore range, as per the specific surface data.

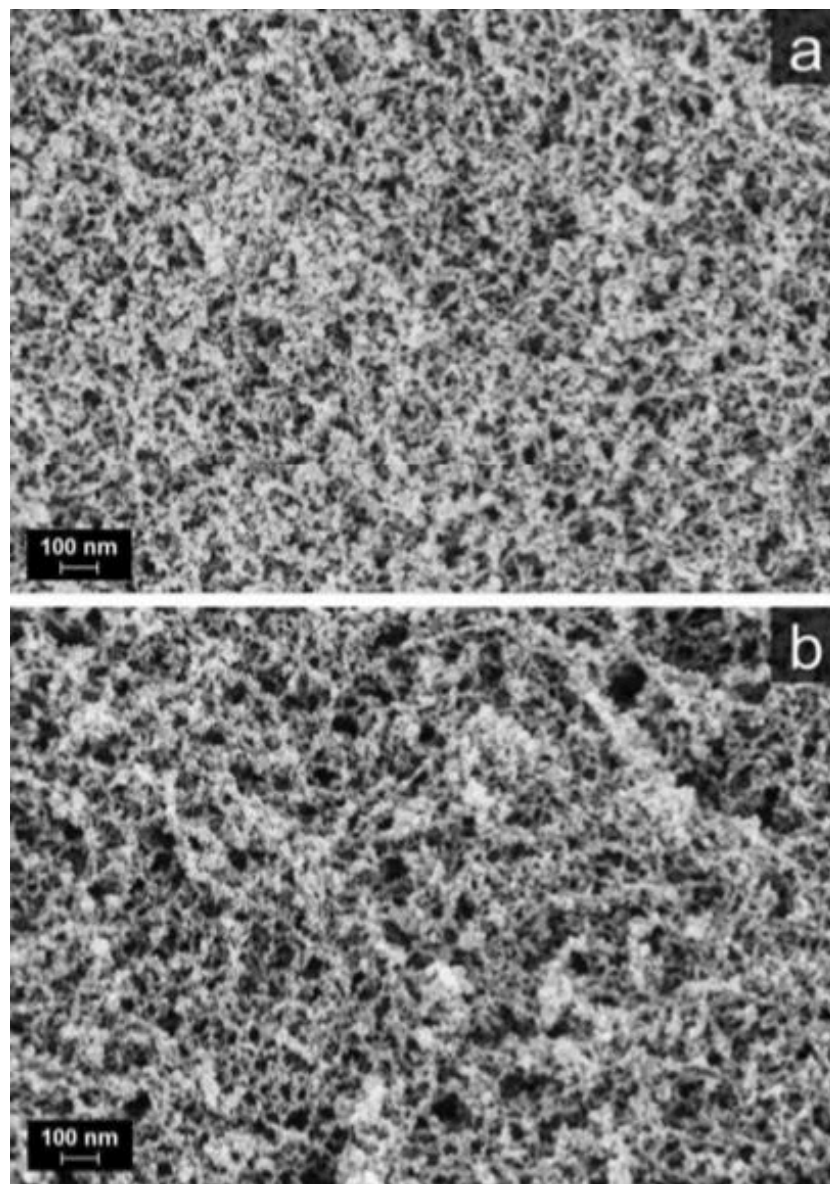


Figure 4.7 SEM images of silica phase in supercritical dried (a) and ambient-dried (b) composite aerogels (Markevicius et al., 2017)

The addition of silylating agent contributed to the preservation of the porous structure in the sample shown in Figure 4.7 by avoiding irreversible pore collapse during ambient pressure drying. Grafting the pore walls with incondensable moieties like silylating agent leads to “spring-back” effect i.e. the repulsion of the grafted groups and elasticity of the solid network caused the re-opening of the pores during the last stage of drying (Mahadik et al., 2012; Wang et al., 2009).

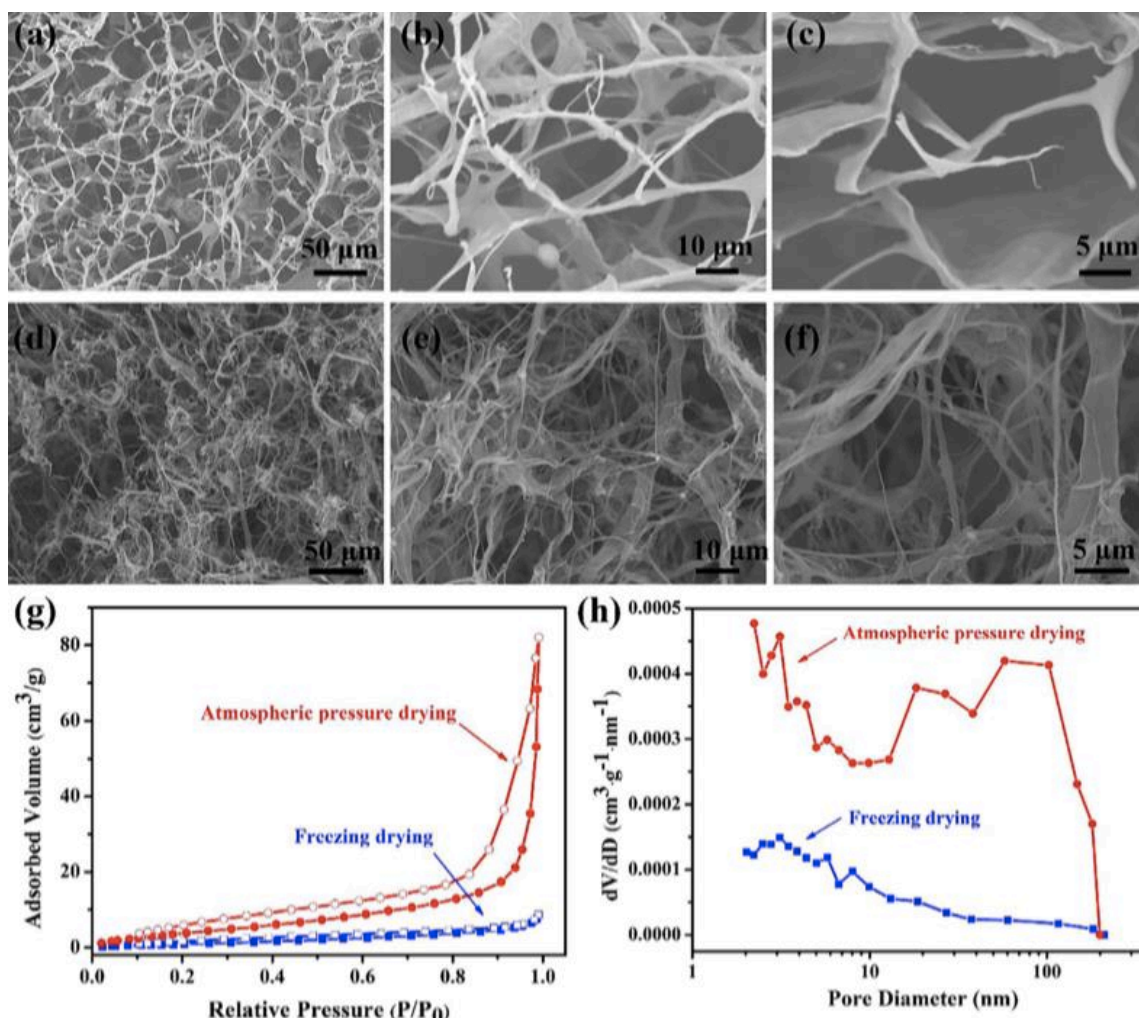


Figure 4.8 (a-c) SEM images of freeze dried cellulose aerogels (d-f) SEM images of atmospheric dried cellulose aerogels (g) Nitrogen adsorption and desorption isotherms and (h) Barret-Joyner-Halenda (BJH) pore size distribution of cellulose aerogel prepared with freeze drying method (blue) and atmospheric pressure drying method (red) (Li et al., 2019).

In another study on the construction of functional cellulose aerogels via atmospheric drying chemically cross-linked and solvent exchanged cellulose nanofibrils by Li et al. (2019)

depicts the microstructure of cellulose aerogel that could be a consistent comparison to starch aerogel. Figure 8 shows the morphology and microstructure of cellulose aerogels observed under SEM. Based on Figure 4.8d-f, ambient dried cellulose aerogels exhibit smaller pore size compared to cellulose aerogel prepared via freeze drying (refer Figure 8a-c). For ambient-dried cellulose aerogels, it is observed that nanofilaments were found ubiquitously in the material. This is due to the freeze-thawing and solvent exchange process that helped to reduce the aggregation and hydrogen bonding between the CNFs (Li et al., 2019). In comparison to the ambient-dried cellulose aerogel, due to the aggregation of CNFs, freeze-dried cellulose aerogels are observed to exhibit pore walls that resembles thin sheets. Li et al. (2019) suggested that the aggregation of CNFs during the freezing process is the result from the growth of ice crystals that would force the CNFs to the crystal boundaries.

Figure 4.8g depicts the result from nitrogen adsorption and desorption isotherm measurement to further investigate the pore structure of the aerogels. From the analysis conducted, it can be observed that both freeze-dried aerogels and ambient-dried aerogels exhibited type IV isotherms with a hysteresis loop at  $P/P_0 > 0.8$  which indicates that both aerogels are mesoporous (Wu et al., 2016). Li et al. (2019) reported that both cellulose aerogels prepared via freeze drying and ambient drying were 4.3 and 22.4  $m^2/g$  respectively according to Brunauer-Emmet-Teller (BET) analysis. Figure 4.8h suggested that ambient-dried aerogels exhibit many mesopores.

Based on the analysis and comparison on the morphology and microstructures of previous studies it can be deduced that the microstructures of ambient-dried starch aerogels are linked to various factors. This includes liquid-vapor interface, incorporation of non-starch ingredient or material and concentration of starch. In order to obtain a porous microstructure of starch aerogel, it is important to take into consideration the attributing factors when synthesizing the material.

#### **4.2.2 Density and shrinkage**

As the sample is proposed to be prepared via ambient pressure drying, the microstructure of aerogel is expected to exhibit low porosity due to structural collapse during evaporative drying and display intermediate density and surface areas. However, it is important to note



that different starch concentration plays a vital role in the display of the material's microstructure. This can be supported by a study conducted by Guerrero-Alburquerque et al. (2020) which highlighted the inverse correlation between chitosan concentration and the linear shrinkage Figure 4.9 for all investigated processing steps (solvent exchanges and drying). This result inferred that as the concentration of starch in the dispersion increases, the shrinkage of aerogel decreases. It is also mentioned that high mechanical strength of more concentrated gels allows them to better withstand the stresses during processing (Guerrero-Alburquerque et al., 2020). In the case of APD (refer to Figure 4.9), it is expected that the aerogels experienced higher shrinkage and it can also be observed that the dependence of shrinkage on chitosan concentration is even more extreme.

Based on Figure 4.9c, the highest density and lowest surface areas are displayed by the APD samples dried at ambient temperature. This sample also showed a substantial scatter in both density and surface area (refer Figure 4.9c). Referring to the same figure, a more consistent result of intermediate densities and highest surface areas are presented by APD samples dried at 65°C. On the other hand, aerogels dried via supercritical carbon dioxide drying display the lowest densities and intermediate surface areas. When comparison is made between aerogels dried via supercritical carbon dioxide drying and ambient pressure drying specifically at 65°C, the surface areas of the APD chitosan aerogels are in similar range as those of SCD. Therefore, when starch aerogels are dried via ambient pressure drying, it is essential to follow similar synthesise process as the chitosan aerogel conducted by Guerrero-Alburquerque et al. (2020) to ensure similar structural integrity, density and surface areas are achievable.

According to Figure 4.9b, it can be observed that when compared two samples dried with ambient pressure drying of different temperatures (i.e. room temperature and 65°C), there is a significant gap in term of the density values. Samples dried via ambient pressure drying at 65°C yield lower density than that of at room temperature. For instance, referring to Figure 9b, 12% of chitosan concentration, aerogels dried via ambient pressure drying yield a density value of about 0.17 g/cm<sup>3</sup> while the other aerogel dried at a room temperature resulted in a density of approximately 0.22 g/cm<sup>3</sup>. It can also be said that the density values of aerogels dried via supercritical drying and ambient pressure drying ay temperature of 65°C are comparable. The density of aerogels dried via supercritical drying is approximately 0.15 g/cm<sup>3</sup> which is slightly lower than that of chitosan. According to

Guerrero-Alburquerque et al. (2020), this phenomenon occur because at a higher APD temperature (i.e. 65°C) result in a faster drying process which reduces the time for which aerogels are exposed to drying induced capillary forces. This subsequently result in less pore collapse and led to higher porosity and density when compared to the aerogels dried at room temperatures for APD.

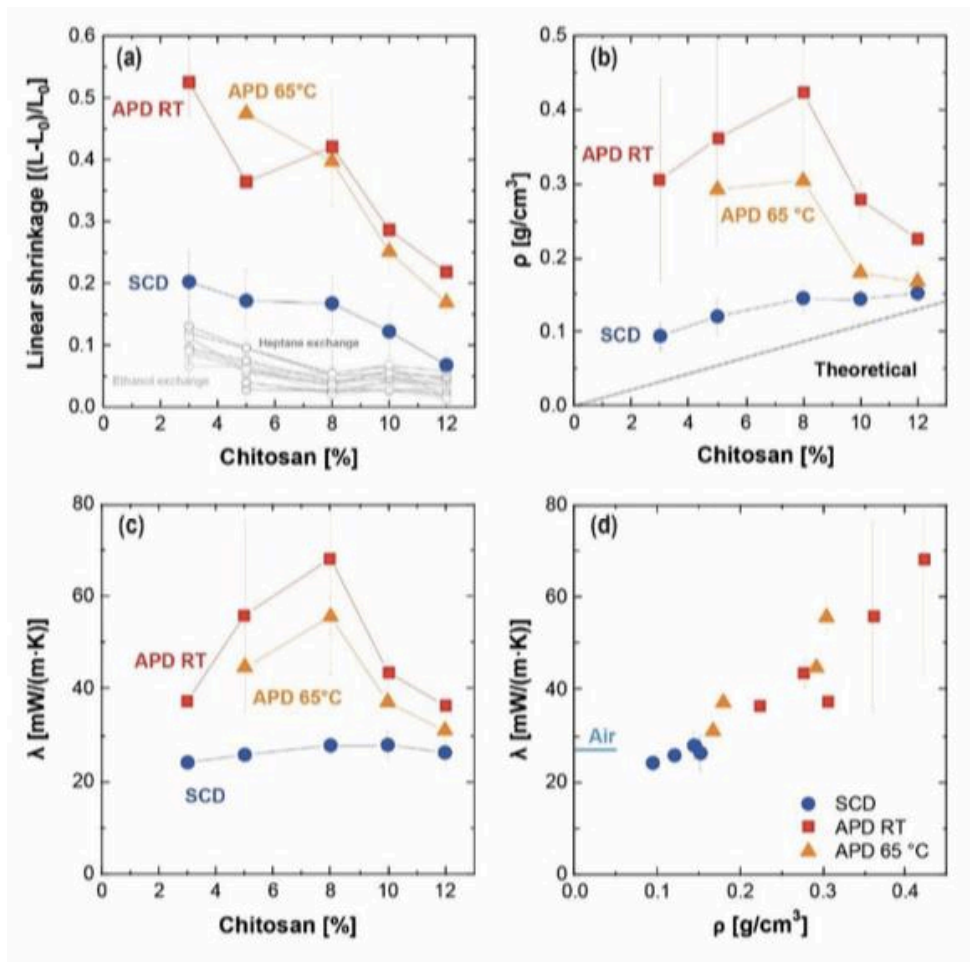


Figure 4.9 (a) Linear shrinkage as a function of chitosan concentration (b) Density dependence on chitosan concentration (c) Thermal conductivity versus chitosan concentration (d) Thermal conductivity versus density (Guerrero-Alburquerque et al., 2020)

According to another study conducted by Ubeyitogullari and Ciftci (2016), the density of the aerogels is greatly influenced by the concentration of starch in the aerogels and the gelatinization temperature of the aerogels. Based on Figure 4.10, a specific trend can be observed. The density of the wheat starch aerogels decreased as the gelatinization temperature increased for all starch concentrations. There was a significant drop of density

at the highest level of starch concentration as the gelatinization temperature was increased to 130°C.

According to Glenn et al. (2008), the significant drop in density is due to the higher gelatinization temperature as more fibrous starch network form at higher gelatinization temperatures. In another similar study conducted by García-González and Smirnova (2013), it is reported that as the concentration of corn starch increased from 7% to 15%, it is observed that the concentration of densities of corn and pea starch aerogels also showing an increasing trend. They also reported that the lowest density obtained was 0.15 g/cm<sup>3</sup> at 7% concentration of starch.

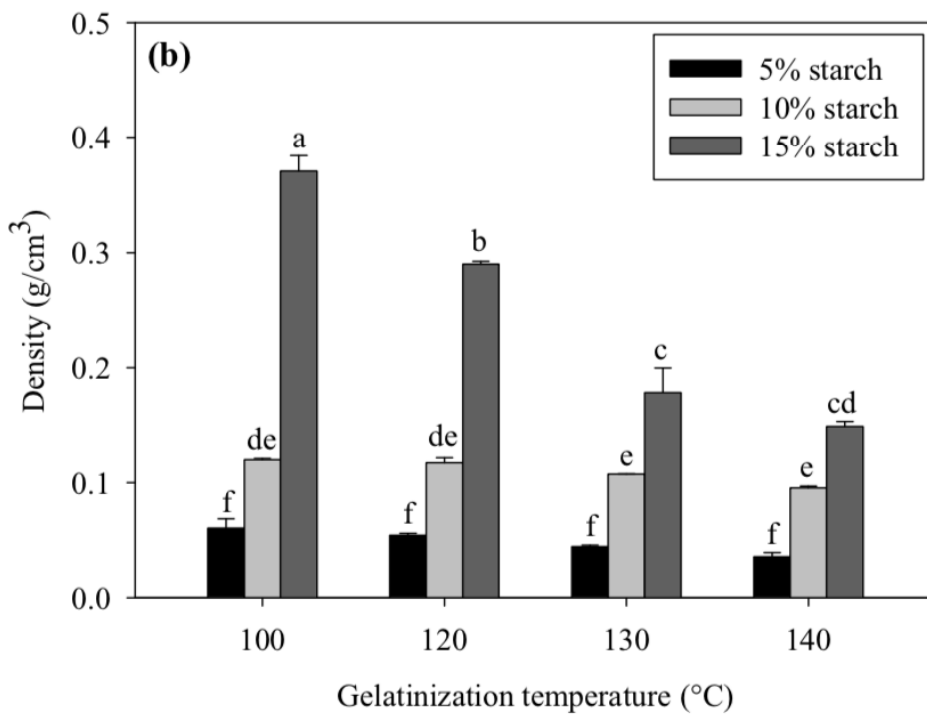


Figure 4.10 Physical Properties; density (g/cm<sup>3</sup>) of wheat starch aerogel monoliths at different gelatinization temperatures and starch concentrations with a mixing rate of 600 rpm (Ubeyitogullari & Ciftci, 2016)

In a study conducted by Markevicius et al. (2017) on “Ambient-dried thermal super insulating monolithic silica-based aerogels with short cellulosic fibers” also reported that shrinkage of aerogel is highly dependent on the concentration fibers in the composite. The decrease of shrinkage occurring during the aging step are usually due to higher fiber

concentration. The movement of mineral chains which takes place during aging is inhibited by the presence of fibers because of the continuation of condensation reaction after sol-gel transition (Markevicius et al., 2017). Markevicius et al. (2017) also stated that shrinkage is also strongly dependent on the mode of drying. Supercritical drying method is usually expected to preserve the volume of the aerogel. Supercritical drying method avoids creating capillary stresses and the total shrinkage of the material occurs essentially during sample drying (Markevicius et al., 2017). Figure 4.11 depicts the difference between total shrinkage of ambient pressure-dried and supercritical-dried aerogels as a function of fiber concentration. During ambient pressure drying, before experiencing a “spring-back” effect, the hydrophobized gel is first contracting due to capillary pressure which subsequently lead to multiple fractures within the gel. Consequently, this creates a loss of monolithic shape which leads to divided beds constituted of granular objects. It is important to note here that the samples keep microscopic monolithic shape in the presence of short cellulose fibers despite internal silica fractionation during evaporative drying (Markevicius et al., 2017).

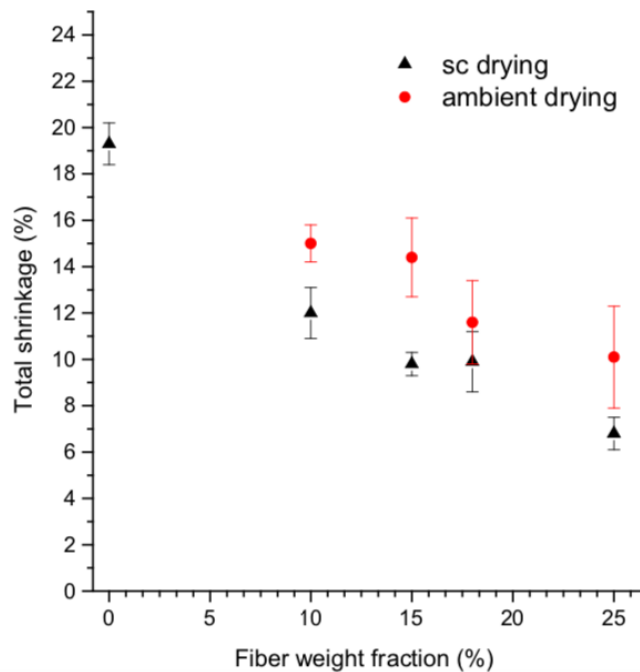


Figure 4.11 Total sample shrinkage as a function of fiber weight fraction for ambient-dried and supercritical-dried aerogels (Monolithic ambient-dried aerogel without addition of fibers is not possible; therefore, the shrinkage of this sample was not determined) (Markevicius et al., 2017).

Based on Figure 4.11, the composite aerogel’s final shrinkage is less than 15 vol%. The shrinkage recorded however is not as drastic as some ambient-dried aerogels synthesized with polymethylsilsesquioxane precursors (PMSQ) as such ambient-dried PMSQ-based aerogels display a linear shrinkage between 40% and 60% prior to linear recovery of 25% as reported by Hayase et al. (2016). However, this study incorporated non-starch material as cross linking agent into the aerogel to improve its mechanical properties which makes this comparison to the starch aerogel consistent.

Table 4.1 Density of several types of aerogel dried via different drying techniques

<b>Aerogel</b>	<b>Density (g/cm<sup>3</sup>)</b>	<b>Drying Mode and Factors</b>	<b>References</b>
Chitosan aerogels	0.17	Ambient pressure drying; optimum higher temperature and chitosan concentration	(Guerrero-Alburquerque et al., 2020)
	0.15	Supercritical carbon dioxide drying; chitosan concentration	
Monolithic silica-based aerogels with short cellulose fibers	0.13	Ambient pressure drying; concentration of fibres	(Markevicius et al., 2017)
Wheat starch aerogels	~ 0.06	Supercritical drying; concentration of starch and the gelatinization temperature	(Ubeyitogullari & Ciftci, 2016)

Cellulose aerogels	0.05882	Ambient pressure (Y. Li et al., 2019) drying; cross linking agent (incorporation of non- starch/cellulose material)
	0.0579	Supercritical drying; cross linking agent (incorporation of non- starch/cellulose material)

From the comparative analysis on previous studies, it can be deduced that there are several factors that govern the density of the starch aerogel. Table 4.1 shows the densities of several types of aerogel dried via different drying techniques. This table also includes the governing factors that corresponds to the densities. This include the incorporation of non-starch material, concentration of starch, gelatinization temperature and the drying technique. However, this study opted for ambient pressure drying, thus, to make the comparison consistent, only the density of aerogels synthesized via ambient pressure drying will be weigh in. The wheat starch aerogel dried via ambient pressure drying is expected to yield density value ranging from 0.1 to 0.2 g/cm<sup>3</sup> based on the governing factors and previous studies of similar scope. The starch aerogel is expected to exhibit the density of similar spectrum as long as the attributing factors that affect the density are taken into heavy consideration during the processing of the material.

#### 4.2.3 Mechanical properties of wheat starch aerogels

The microstructure of starch based aerogels are linked with its mechanical properties (García-González et al., 2012; Glenn & Iriving, 1995; Zhang et al., 2017). On a pilot study conducted by Glenn and Iriving (1995) showed a positive correlation between the densities of starch aerogels and foams with the elasticity and compressive strength. Since density

affects the mechanical properties of starch based aerogel, it is safe to deduce that the concentration level of starch in starch based aerogel plays a huge role in attributing to its mechanical properties. This statement can be supported by a review conducted by Zhu (2019) stated that the amylose content of starch is crucial in determining the mechanical properties of the resulting aerogel.

In a study conducted by Ganesan et al. (2016) on cellulose aerogels, both samples obtained from solvent exchange using isopropanol and ethanol present varying compressive deformation. Based on Figure 4.12, both samples exhibit uniform linear-elastic region under static loading. However, both sample started to show different pattern in the plastic collapse under static loading. From the stress-strain curve shown in Figure 4.12, the plastic yield curve displayed by the sample from ethanol showed a rough pattern. Unlike the sample from ethanol, the samples from isopropanol display a smooth plastic yield curve; due to the packing of nanofibrils and higher volume fraction of solid on the cell wall and the pore size distribution (Ganesan et al., 2016). This inference can also be supported by a report published by Glenn and Irving (1995) which stated that a weak mechanical properties of starch aerogels are contributed by uneven distribution of the pores and irregularity of the pore size .

Table 4.2 Summary of mechanical properties of cellulose materials (Ganesan et al., 2016).

<b>Sample</b>	<b>Young's Modulus, <math>E_o</math> (MPa)</b>	<b>Yield stress at 1% strain <math>\sigma_o</math> (kPa)</b>	<b>Poisson ratio, <math>\nu</math></b>	<b>Relative density (<math>\rho_o/\rho_s</math>)</b>	<b>Energy absorption up to 40% of strain (kJ/m<sup>3</sup>)</b>
Isopropanol	30.55 ± 1.55	1783 ± 5	0.33	0.189	101.92 ± 3.0
Ethanol	49.3 ± 0.6	8747 ± 358	Fractured	0.321	286.78 ± 3.8

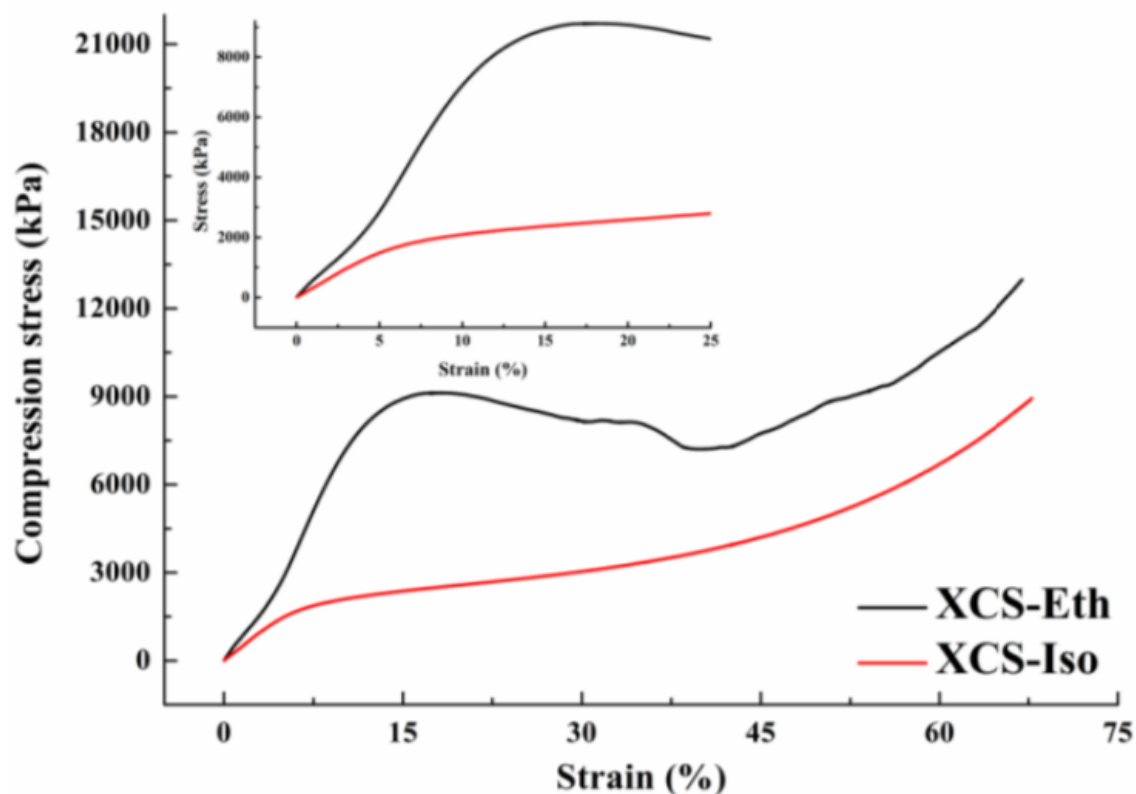


Figure 4.12 The stress-strain curve of cellulose scaffolds (Ganesan et al., 2016).

In comparison to samples from isopropanol, samples derived from ethanol presented a fracture after reaching the ultimate strain at about 18% of strain. The fracture is suspected to occur due to inhomogenous distribution of micropores and tightly bound nanofibrils in the cell walls which shows less surface area. According to Glenn and Irving (1995), weak mechanical strength of starch aerogels are contributed by uneven distribution of pores, irregularity of the pore size and the starch granule remnants. After the sample reaches 18% of strain, the cell walls can be crushed locally at some parts of the sample. From this point onwards, the material is expected to continue to experience plastic collapse. The yield stress of the samples obtained from ethanol is higher than that of isopropanol. This is due to the large difference in relative density and the pore and nanofibril distribution in the cell walls of the material.



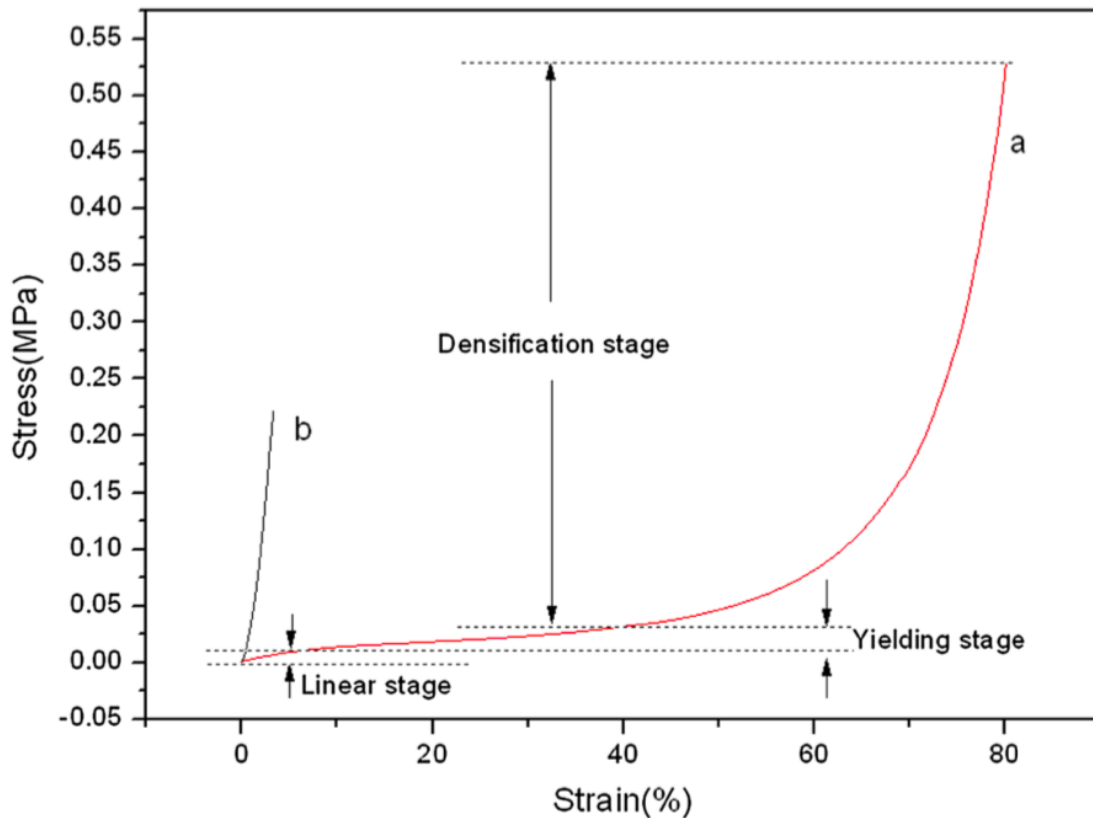


Figure 4.13 The stress-strain curves at 25°C of (a) the starch-enhanced melamine-formaldehyde (SEMF) aerogel and (b) pure melamine-formaldehyde (MF) aerogel (Zhang et al., 2017).

The mechanical properties of starch aerogels are also linked to incorporation of non-starch ingredients. The mechanical properties of starch based aerogels can be significantly improved with the incorporation of non-starch ingredient. In a study conducted by Ago et al. (2016), the Young's modulus and yield stress showed a significant increment in compression mode of starch composite aerogel through increasing the cell wall thickness by incorporating nanofibril. In term of mchanical properties, starch nanofibril composite foams were similar to polystyrene foams (Ago et al., 2016). Composite melamine-formaldehyde aerogels with the addition of starch presented better mechanical durability and elasticity in comparison to melamine-formaldehyde aerogels. According to Zhang et al. (2017) the incorporation of starch in the aerogels resulted in a more reinforced network of the hybrid aerogel while helping to reduce the relaxation of the polymer chains.

According to Zhang et al. (2017), based on Figure 4.13b, pure malamine-formaldehyde aerogel can only withstand strain of  $\sim 4\%$  and stress of  $\sim 0.225\text{MPa}$ . In comparison with SEMF curve (refer Figure 4.13a), it can be divided into three phases to the slope namely the linear stage, the yielding stage and the densification stage. In the linear stage, the compression curve slope remained the same with a strain range from 0% to about 5%. In the plastic deformation region, the stress ranges from 5% to about 40%. In this stage, it can be seen that the stress increased at a fixed rate lower than that of the first stage. However, in the last stage (inelastic hardening also known as densification stage) of strain higher than 40%, as the strain increase, the stress-strain curve also increases. Therefore, based on the analysis above it can be deduced that the high mechanical properties of SEMF aerogel compared to pure MF could be attributed to the native toughness of starch and the size of broadening of the porous structure.

In another study of construction of functional cellulose aerogels via atmospheric drying chemically cross-linked and solvent exchanged cellulose nanofibrils conducted by Li et al. (2019), the evaluation of the mechanical properties for both aerogels prepared via freeze drying and ambient drying are depicted through the compression stress-strain curves. As shown in Figure 4.14a, both aerogels prepared via freeze drying and ambient pressure drying undergo compression up to 50% of their original thickness. From the stress-strain curve shown, compression stress for freeze-dried aerogels is higher than that of ambient-dried aerogel noting that both aerogels exhibit similar density i.e. freeze-dried aerogel:  $57.9\text{ mg/cm}^3$  and ambient-dried aerogel  $58.82\text{ mg/cm}^3$  (Li et al., 2019). According to Jimenez et al. (2016), the relatively high resistance to compression in the aerogel process was due to the aggregation of CNFs in the freeze-dried aerogel which led to the sheet like morphology of the pore walls. For atmospheric-dried aerogel, the compression stress values presented are lower for the same compression strain values. This can be inferred to the nanofilament skeleton morphology which translates to weaker pore walls (Erlandsson et al., 2018; Jimenez et al., 2016).

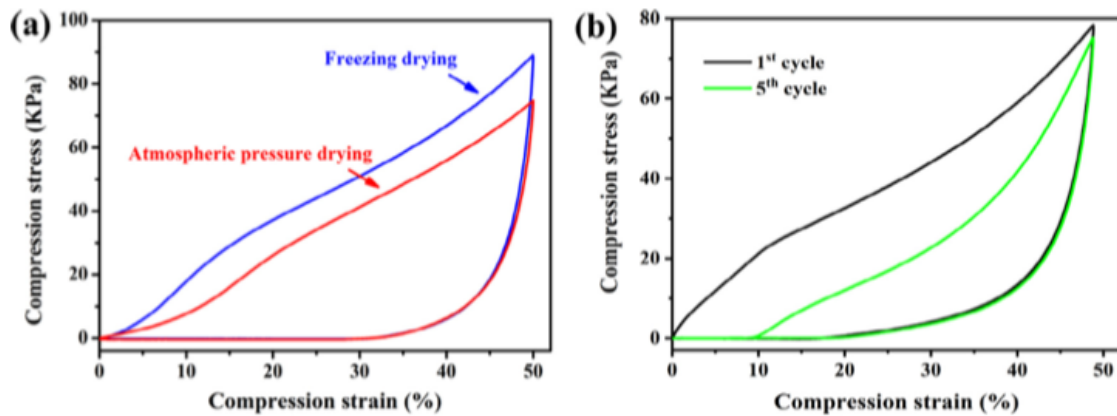


Figure 4.14 (a) Compression strain-stress of cellulose aerogels prepared with freeze drying method and ambient pressure drying (b) 5 cyclic fatigue compression strain-stress test with a compression of 50% (Li et al., 2019).

Both freeze-dried and atmospheric-dried aerogels presented excellent thickness recovery despite the difference, showing 70% recovery of their original thickness after the compressive stress was removed as shown from the hysteresis of the stress-strain curve. Figure 4.14b demonstrated the flexibility of the atmospheric-dried aerogels as it was subjected with hysteresis tests with compression strain of 50%. Despite subjected to five cycles of hysteresis tests, the aerogels were observed to be in good shape recovery ability and flexibility while maintaining over 91% of its original height although the maximum compression stress showed a minor decrease (Li et al., 2019). This demonstrates that cross-linking could enhance the mechanical properties of cellulose aerogels.

Based on the comparison and analysis conducted on the mechanical properties from different types of aerogels ranging from cellulose-based aerogel to starch-enhanced melamine formaldehyde aerogels, it can be concluded that the mechanical properties of starch-based aerogel depend on several factors. The factors include the incorporation of non-starch ingredients as cross-linking agents, the concentration of starch and the type of liquid-vapor interface. It is also worthy to note that an enhancement in the mechanical properties will compromise other functionalities of starch aerogels (Zhu, 2019). Therefore, it is crucial to optimize the mechanical properties of starch aerogels in relation to specific application. Therefore, the wheat starch aerogel is forecasted to exhibit similar mechanical properties with the study conducted by Ganesan et al., (2016) as the attributing factors are similar with the one proposed in this review paper.

#### 4.2.4 Thermal Conductivity of Starch-based Aerogel

According to Fricke (1986), the thermal conductivity of a porous material like aerogel could be categorized into three contributions namely the conduction of the solid network, radiation through or within the pores and the conduction of the gaseous phase. As the porosity increases, the contribution of solid network decreases. This can be inferred to the restriction of the propagation of phonons in the aerogel backbone as a result of the large quantity of pores (Fricke & Emmerling, 1992). The contribution of the gaseous phase is due to the elastic collision between gas molecules. As stated by Illera et al. (2018), the mean free path of the gas molecules enclosed in the pores and the pore sizes affect the thermal conductivity in the gaseous phase. To achieve this, the presence of pore sizes below the mean free path of air molecules subsequently inhibit the thermal diffusion of the gas. This statement basically explains the basic idea of the Knudsen Effect. Therefore, this factors into the superinsulating properties of the aerogels. One of the major applications of aerogels is thermal insulation (Druel et al., 2017; Glenn & Irving, 1995; Wang et al., 2018). A pilot study on starch aerogel conducted by Glenn and Irving (1995) suggested that the thermal conductivity of commercial insulation samples was similar to that of starch-based aerogels. According to Druel et al. (2017), the thermal conductivity of starch-based aerogels are linked to the type of starch and the processing condition. Therefore, there are several factors that govern the thermal conductivity of starch-based aerogels.

In a typical aerogels, low thermal conductivity of solid skeleton and gaseous occupied pores usually resulted in a very low thermal conductivity. Thus, it can be deduced that thermal conductivity is directly proportional to the size of pores (thermal conductivity of aerogels decreases as the pores size decreases) as pores of smaller size limit free path of air particles (pores with a size less than 70 nm) (Jiménez-Saelices et al., 2018). Table 4.2 presents the thermal conductivity values of aerogels prepared from different drying methods from previous reports. A study carried out by Markevicius et al. (2017) suggested that different types of cellulose fibers and concentration of cellulose fibers induced the possible modification of silica sol pH which subsequently affect the morphology of the aerogel towards a more colloidal internal structure and potentially affect the thermal conductivity of the aerogels. This is an interesting example to demonstrate the intricate relationship between several factors that could affect the thermal properties of aerogels.

Figure 4.15 shows the thermal conductivity of ambient-dried and supercritical-dried aerogels. For both cases, there is an increasing trend observed at which the increment of fiber concentration in the aerogels resulted in a slight increment of thermal conductivity of no more than 0.004 W/mK. It can be said that the increment in the thermal conductivity value is not surprising as the bulk density of the composite aerogels increases with the increase of fiber fraction or fiber concentration. It can also be observed that thermal conductivity of ambient-dried aerogel were slightly higher than that of supercritical-dried aerogel. Markevicius et al. (2017) inferred that the high values of thermal conductivity in the ambient-dried aerogel were most likely due to the macroscopic cracks during the ambient drying at which they were too large to take advantage of the Knudsen effect.

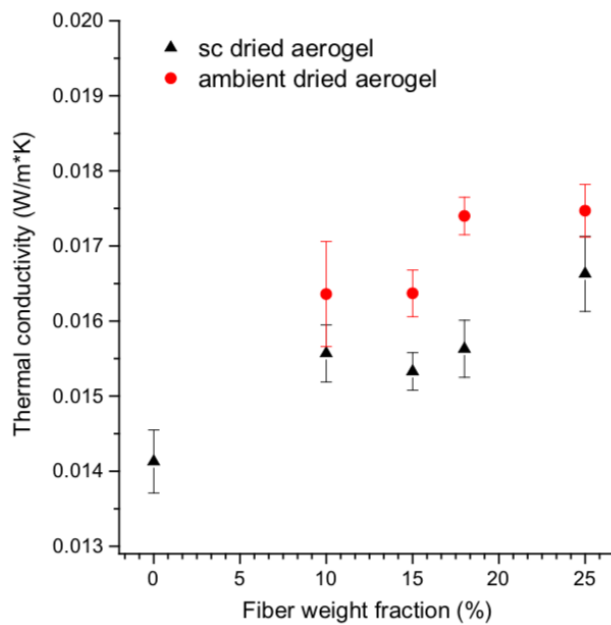


Figure 4.15 Thermal conductivity of Tencel fiber-silica composite aerogels prepared via ambient pressure drying and supercritical drying (Markevicius et al., 2017)

In a study conducted by Li et al. (2017) on improved mechanical and thermal insulation properties of monolithic attapulgite nanofiber/silica aerogel composite dried at ambient pressure showed a correlation between incorporation of reinforcement material, attapulgite (ATP) in monolithic silica aerogel composites exhibiting ultralow density and excellent thermal insulation properties. Based on Figure 4.15, as the content of ATP fibers rises, the thermal conductivity increases in the range of 0.0198 – 0.0228 Wm<sup>-1</sup>K<sup>-1</sup>. As known, generally the thermal conductivity of a porous material can be classified into three

categories which are the thermal transportation by the solid phase, gas phase and radiation. Under ambient condition, the conductive thermal transportation through bulk solid skeleton is the dominant contribution for mesoporous aerogels, where as the dominance for gaseous and radiation thermal is significance only at elevated temperature (Scheuerpflug et al., 1985). Therefore, the addition of ATP in the small amount contributed to the high porosity which led to the decrease in the bulk density as shown in Table xx. Hence, this can be inferred to the decrease of thermal conductivity in aerogel. Based on Figure 4.16, it is evident that with the increase of ATP concentration in the matrix attributed to the thermal conductivity of the matrix. As shown Figure 4.16, the increment of fiber concentration increases the conductive heat transfer. According to Li et al. (2017), the ATP fibers help to reinforce the silica network and act as additional heat transfer passageways through the fiber structure when subjected to a temperature gradient. Consequently, with strengthened the heat transfer through the bulk solid skeleton resulted in the high thermal conductivity.

Table 4.3 Physical and textural properties of silica with different content of ATP fibers (Li et al., 2017)

<b>ATP (wt %)</b>	<b>Bulk density (g/cm<sup>3</sup>)</b>	<b>Porosity (%)</b>	<b>Surface area (m<sup>2</sup>/g)</b>	<b>Pore volume (cc/g)</b>	<b>Mean pore size (nm)</b>	<b>Linear shrinkage (%)</b>
<b>0</b>	0.188	83.6	947.8	2.87	12.1	32.3
<b>1</b>	0.163	85.8	930.7	2.80	12.1	19.2
<b>2</b>	0.173	84.9	926.4	2.75	12.2	17.5
<b>5</b>	0.180	84.3	890.3	2.72	12.3	16.1
<b>10</b>	0.185	83.9	830.1	2.71	12.4	13.3
<b>20</b>	0.192	83.3	790.2	2.50	12.8	10.2

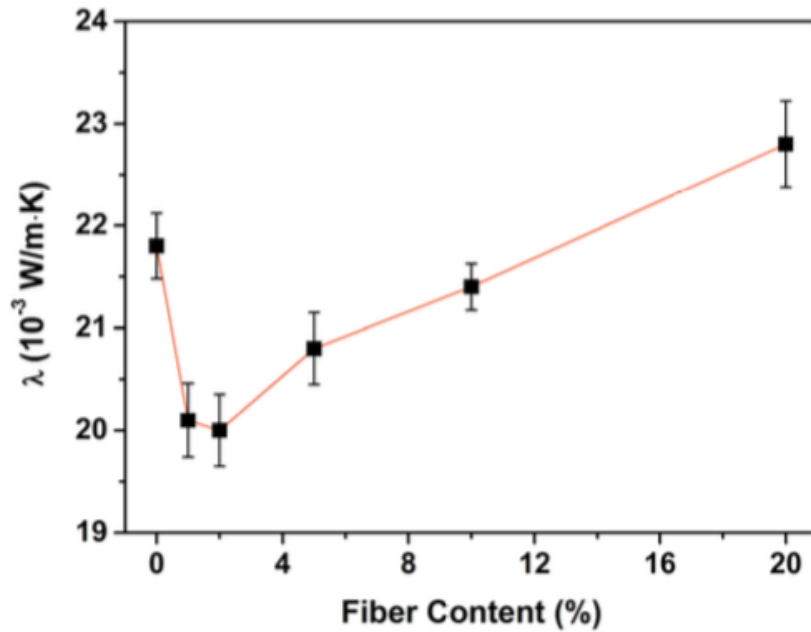


Figure 4.16 The effect of fiber content on thermal conductivity of the ATP/silica aerogel composite (Li et al., 2017)

Table 4.4 Thermal conductivity of several types of aerogel dried via different drying techniques

<b>Aerogel</b>	<b>Drying Method</b>	<b>Thermal conductivity (<math>Wm^{-1}K^{-1}</math>)</b>	<b>References</b>
Recycled cellulose aerogel	Freeze drying	0.032	(Duong et al., 2018)
Polyethylene glycol-Cellulose aerogel	Freeze drying	0.24	(Yang et al., 2016)
Cellulose-carbon nanotube aerogel	Freeze drying	0.01 – 0.11	(Gnanaseelan et al., 2018)
Silica-carbon nanotube aerogel	Supercritical drying	0.004 – 0.03	(Sun et al., 2014)
Silica aerogel	Freeze drying	0.045 – 0.07	(Maleki et al., 2018)
Nano fibrillated cellulose aerogel	Freeze drying	0.0251 – 0.0346	(Gupta et al., 2018)
Melamine sponge – silica aerogel	Microwave drying	0.03 – 0.04	(Guo et al., 2019)

Novel cellulose aerogel	Ambient drying	pressure	0.0417	(Ebrahimi et al., 2020)
Chitosan-urea aerogel	Ambient drying	pressure	0.0309	(Guerrero- Alburquerque et al., 2020)

Based on Table 4.3, it can be seen that cellulose aerogel dried via ambient pressure drying presented about similar values in contrast to other cellulose aerogels fabricated via supercritical drying, freeze drying and microwave drying. Therefore, without the need of sophisticated equipment, the aerogel sample fabricated via ambient pressure drying presented comparable values of thermal conductivity. From this comparison and analysis, it can also be deduce that improving the mechanical properties of starch-based aerogel may compromise the thermal conductivity of the material. By the mean of increasing the concentration of starch in the aerogel will result in better mechanical properties which also lead to an increase in the density of the material. Consequently leading to higher thermal conductivity of aerogels. Thus, the wheat starch aerogel is forecasted to exhibit thermal conductivity of ranging 0.03 to 0.05  $Wm^{-1}K^{-1}$  by weighing in governing factors based on similar previous studies.



## **CHAPTER 5**

### **CONCLUSION AND FUTURE RESEARCH DIRECTIONS**

This review presented the main results obtained until now mainly on cellulose aerogels made via ambient pressure drying. Due to limited studies on starch aerogels fabricated via this drying route, studies on cellulose aerogels dried via ambient pressure drying are opted due to similarities in terms of their chemical structures between cellulose and starch to make this review and the potential outcome consistent. This review also included the properties and morphology of starch and cellulose aerogels compared to those of the classical aerogels (inorganic and synthetic polymer) synthesized via conventional methods like supercritical carbon dioxide drying and freeze drying. In general, starch aerogels and other bio-aerogels (i.e. cellulose aerogel, pectin aerogel) are considered to be very “young” and emerging materials. Due to the fact that this material has the interface of different disciplines that were previously non-crossing, there are numerous open questions to be answered. In order to explore the multi-disciplinary approach of this material, it is essential to understand the properties of starch aerogels and how they are influenced by the intricacy of attributing factors as discussed in Chapter 4.

In the production procedures of starch aerogels, retrogradation and starch gelatinization for hydrogel formation are commonly used routes. Alcogel is then formed through organic solvent exchange. The alcogel is then dried using either freeze drying or supercritical carbon dioxide drying to produce porous and low-density starch aerogels. Therefore, this paper reviews the possibility of fabricating aerogel via ambient pressure drying (APD) in the light of upscaling and commercialization purpose of this material. Other than cost effective and reduce production time compared to the conventional routes, this approach will also have less impact on the environment as it utilizes less hazardous chemical in the production process. The environmental impacts of manufacturing starch aerogels can be

significantly reduced by optimizing formulations and processing conditions of the starch aerogels.

This review also analyses the critical parameters describing the properties of starch aerogels dried via this route namely the microstructure and morphology, density and shrinkage, mechanical properties and thermal conductivity. These functionalities are tunable by means of varying preparation conditions (i.e. type of starch, drying methods and initial starch concentration), drying temperature, incorporation of non-starch material and surface modifications. From the comparative analysis done on these parameters, it is found that these parameters are intricately correlate to each other in the function of the preparation conditions. Therefore, varying the preparation condition yields varying results tunable to the desired application. It is clear that starch aerogels need a multidisciplinary approach and common effort of the experts from different scientific fields.

Numerous options of starch derivatization and functionalization may open new starch aerogel applications which remain unexplored. Therefore, there are copious research opportunities to understand and utilize starch aerogels. To do this, establishing the structure function relationship (like mechanical properties of the starch aerogels) of the components of the aerogels is essential. A precise establishment should be executed appropriately on the effect of type of starch used and its modification, the processing methods which often includes the type of solvent type (especially for solvent exchange process; i.e. finding appropriate solvent with optimum polarity and less hazardous) and drying conditions on the properties of starch aerogels. To achieve desired functionalities (catering to the application), the effect of incorporation of non-starch ingredients or materials into the starch aerogel should be studied further for future development. On the same capacity, a study on molecular level on the relationship and interaction between starch and the incorporated non-starch material in this composite during its processing.

# QUESTIONS AND ANSWERS

## **1. What is the difference between the aerogels as proposed in this paper compared to the ones listed in Chapter 2 Literature Review?**

The processing route mainly sets apart between the aerogels listed in literature review and the starch aerogels proposed in this paper. This paper opted a different drying route which is ambient pressure drying compared to other conventional drying mechanisms which are supercritical carbon dioxide drying and freeze drying. To date, there are a limited amount of studies which synthesized aerogels via ambient pressure drying. In order to bridge this gap, this processing route is opted other than its green processing requirement which do not demand sophisticated equipment and less chemicals involved. Ambient pressure drying is also opted to see the feasibility of commercialization of aerogels via this route due to its overall economical production cost compared to other drying routes.

## **2. What are the factors that affecting properties of starch aerogels?**

There are several prime parameters as highlighted by this paper namely the morphology and microstructure of aerogels, density and shrinkage, mechanical properties and thermal conductivities. Based on previous studies, there several factors that govern these parameters for ambient pressure dried aerogels. The factors are;

- i. The concentration of starch in the dispersion
- ii. The gelatinization temperature
- iii. The incorporation of non-starch material (as cross-linking agents)
- iv. The incorporation of surface modification agents

It is crucial to understand that these parameters are highly dependable with the aforementioned factors and the parameters are intricately correlate to one another in the function of the preparation conditions. Therefore, varying the preparation condition yields varying results tunable to the desired application.

## REFERENCES

- Abhari, N., Madadlou, A., & Dini, A. (2017). Structure of starch aerogel as affected by crosslinking and feasibility assessment of the aerogel for an anti-fungal volatile release. *Food Chemistry*, *221*, 147–152.
- Aegerter, M. A., Leventis, N., & Koebel, M. M. (Eds.). (2011). *Aerogels Handbook*.
- Ago, M., Ferrer, A., & Rojas, O. J. (2016). Starch-Based Biofoams Reinforced with Lignocellulose Nanofibrils from Residual Palm Empty Fruit Bunches: Water Sorption and Mechanical Strength. *ACS Sustainable Chemistry & Engineering*, *4*(10), 5546–5552.
- Ahmadi, M., Madadlou, A., & Saboury, A. A. (2016). Whey protein aerogel as blended with cellulose crystalline particles or loaded with fish oil. *Food Chemistry*, *196*, 1016–1022.
- Ahmed, M. S., & Attia, Y. A. (1995). Aerogel materials for photocatalytic detoxification of cyanide wastes in water. *Journal of Non-Crystalline Solids*, *186*, 402–407.
- Alkemper, J., Buchholz, T., Murakami, K., & Ratke, L. (1995). Solidification of aluminium alloys in aerogel moulds. *Journal of Non-Crystalline Solids*, *186*, 395–401.
- Anas, M., Gönel, A. G., Bozbag, S. E., & Erkey, C. (2017). Thermodynamics of Adsorption of Carbon Dioxide on Various Aerogels. *Journal of CO2 Utilization*, *21*, 82–88.
- Aravind, P. R., Shajesh, P., Soraru, G. D., & Warriar, K. G. K. (2010). Ambient pressure drying: a successful approach for the preparation of silica and silica based mixed oxide aerogels. *Journal of Sol-Gel Science and Technology*, *54*(1), 105–117.
- Bakierska, M., Chojnacka, A., Świątosławski, M., Natkański, P., Gajewska, M., Rutkowska, M., & Molenda, M. (2017). Multifunctional Carbon Aerogels Derived by Sol–Gel Process of Natural Polysaccharides of Different Botanical Origin. *Materials*, *10*(11), 1336.
- Bangi, U. K. H., Lee, K.-Y., Maldar, N. M. N., & Park, H.-H. (2018). Synthesis and Properties of Metal Oxide Aerogels via Ambient Pressure Drying. *Journal of Nanoscience and Nanotechnology*, *19*(3), 1217–1227.
- Biener, J., Stadermann, M., Suss, M., Worsley, M. A., Biener, M. M., Rose, K. A., & Baumann, T. F. (2011). Advanced carbon aerogels for energy applications. *Energy and Environmental Science*, *4*(3), 656–667.

- Błaszczczyński, T., Ślosarczyk, A., & Morawski, M. (2013). Synthesis of silica aerogel by supercritical drying method. *Procedia Engineering*, 57, 200–206.
- Conway, B. E. (1991). Transition from “supercapacitor” to “battery” behavior in electrochemical energy storage. *Proceedings of the International Power Sources Symposium*, 138(6), 319–327.
- da Silva, A., Donoso, P., & Aegerter, M. A. (1992). Properties of water adsorbed in porous silica aerogels. *Journal of Non-Crystalline Solids*, 145(C), 168–174.
- Darpenigny, C., Nonglaton, G., Bras, J., & Jean, B. (2019). Highly Absorbent Cellulose Nanofibrils Aerogels Prepared by Supercritical Drying Clémentine. *Sensors & Actuators: B. Chemical*, (October), 127065.
- Davis, P. J., Jeffrey Brinker, C., Smith, D. M., & Assink, R. A. (1992). Pore structure evolution in silica gel during aging/drying II. Effect of pore fluids. *Journal of Non-Crystalline Solids*, 142, 197–207.
- Demilecamps, A., Beauger, C., Hildenbrand, C., Rigacci, A., & Budtova, T. (2015). Cellulose–silica aerogels. *Carbohydrate Polymers*, 122, 293–300.
- Deshpande, R., Smith, D. M., & Jeffrey Brinker, C. (1996). *Patent No. US 5565142*. United States.
- Druel, L., Bardl, R., Vorwerg, W., & Budtova, T. (2017). Starch Aerogels: A Member of the Family of Thermal Superinsulating Materials. *Biomacromolecules*, 18(12), 4232–4239.
- Duong, H. M., Liu, P., Nguyen, T. X., Nguyen, S. T., Feng, J., & Cheng, H. (2018). Cellulose and Protein Aerogels for Oil Spill Cleaning, Life Science and Food Engineering Applications. *RSC Green Chemistry*, 2018-Janua(58), 228–260.
- Ebrahimi, A., Dahrazma, B., & Adelifard, M. (2020). Facile and novel ambient pressure drying approach to synthesis and physical characterization of cellulose-based aerogels. *Journal of Porous Materials*, 27(4), 1219–1232.
- El-Naggar, M. E., Othman, S. I., Allam, A. A., & Morsy, O. M. (2020). Synthesis, drying process and medical application of polysaccharide-based aerogels. *International Journal of Biological Macromolecules*, 145, 1115–1128.
- Erlandsson, J., Pettersson, T., Ingverud, T., Granberg, H., Larsson, P. A., Malkoch, M., & Wågberg, L. (2018). On the mechanism behind freezing-induced chemical crosslinking in ice-templated cellulose nanofibril aerogels. *Journal of Materials Chemistry A*, 6(40), 19371–19380.
- Feinle, A., & Hüsing, N. (2015). Mixed metal oxide aerogels from tailor-made precursors.

*Journal of Supercritical Fluids*, 106.

- Filipe, I. (2015). *Extended Abstract Environmental impact of thermal renders*.
- Fricke, J. (1986). *Thermal Transport in Porous Superinsulations*.
- Fricke, J. (1988). Aerogels — highly tenuous solids with fascinating properties. *Journal of Non-Crystalline Solids*, 100(1–3), 169–173.
- Fricke, Jochen, & Emmerling, A. (1992). Aerogels. *Journal of the American Ceramic Society*, 75(8), 2027–2035.
- Ganesan, K., Dennstedt, A., Barowski, A., & Ratke, L. (2016). Design of aerogels, cryogels and xerogels of cellulose with hierarchical porous structures. *Materials and Design*, 92, 345–355.
- Ganobjak, M., Brunner, S., & Wernery, J. (2019). Aerogel materials for heritage buildings: Materials, properties and case studies. *Journal of Cultural Heritage*.
- García-González, C. A., Alnaief, M., & Smirnova, I. (2011). Polysaccharide-based aerogels—Promising biodegradable carriers for drug delivery systems. *Carbohydrate Polymers*, 86(4), 1425–1438.
- García-González, C. A., Camino-Rey, M. C., Alnaief, M., Zetzl, C., & Smirnova, I. (2012). Supercritical drying of aerogels using CO<sub>2</sub>: Effect of extraction time on the end material textural properties. *The Journal of Supercritical Fluids*, 66, 297–306.
- García-González, C. A., Jin, M., Gerth, J., Alvarez-Lorenzo, C., & Smirnova, I. (2015). Polysaccharide-based aerogel microspheres for oral drug delivery. *Carbohydrate*
- García-González, C. A., & Smirnova, I. (2013). Use of supercritical fluid technology for the production of tailor-made aerogel particles for delivery systems. *The Journal of Supercritical Fluids*, 79, 152–158.
- García, A. M., Budarin, V. L., Zhou, Y., De bruyn, M., Hunt, A. J., Lari, L., ... Shuttleworth, P. S. (2018). Monolithic mesoporous graphitic composites as super capacitors: from Starbons to Starenes®. *Journal of Materials Chemistry A*, 6(3), 1119–1127.
- Glenn, G. M., & Irving, D. W. (1995). Starched-based microcellular foams. *Cereal Chemistry*, 155–161.
- Glenn, Gregory M., Klamczynski, A., Chiou, B.-S., Orts, W. J., Imam, S. H., & Wood, D. F. (2008). Temperature Related Structural Changes in Wheat and Corn Starch Granules and Their Effects on Gels and Dry Foam. *Starch - Stärke*, 60(9), 476–484.
- Gnanaseelan, M., Chen, Y., Luo, J., Krause, B., Pionteck, J., Pötschke, P., & Qi, H. (2018). Cellulose-carbon nanotube composite aerogels as novel thermoelectric materials.

- Composites Science and Technology*, 163, 133–140.
- Guerrero-Alburquerque, N., Zhao, S., Adilien, N., Koebel, M. M., Lattuada, M., & Malfait, W. J. (2020). Strong, Machinable, and Insulating Chitosan-Urea Aerogels: Toward Ambient Pressure Drying of Biopolymer Aerogel Monoliths. *ACS Applied Materials and Interfaces*, 12(19), 22037–22049.
- Guo, T., Chen, R., Wu, S., Zhang, L., Yun, S., Zhang, J., ... Huang, A. (2019). Fast microwave dried mechanical robust melamine sponge/methyltrimethoxysilane-based silica aerogel composites with bendability and superhydrophobicity. *Journal of Porous Materials*, 26(5), 1369–1375.
- Gupta, P., Singh, B., Agrawal, A. K., & Maji, P. K. (2018). Low density and high strength nanofibrillated cellulose aerogel for thermal insulation application. *Materials & Design*, 158, 224–236.
- Habibi, Y., Lucia, L. A., & Rojas, O. J. (2010). Cellulose Nanocrystals: Chemistry, Self-Assembly, and Applications. *Chemical Reviews*, 110(6), 3479–3500.
- Hammami, C., & René, F. (1997). Determination of Freeze-drying Process Variables for Strawberries. *Journal of Food Engineering*, 32(2), 133–154.
- Hayase, G., Kanamori, K., Maeno, A., Kaji, H., & Nakanishi, K. (2016). Dynamic spring-back behavior in evaporative drying of polymethylsilsesquioxane monolithic gels for low-density transparent thermal superinsulators. *Journal of Non-Crystalline Solids*, 434, 115–119.
- Herrmann, G., Iden, R., Mielke, M., Teich, F., & Ziegler, B. (1995). On the way to commercial production of silica aerogel. *Journal of Non-Crystalline Solids*, 186, 380–387.
- Hrubesh, L. W. (1998). Aerogel applications. *Journal of Non-Crystalline Solids*, 225(1–3), 335–342.
- Hüsing, N., & Schubert, U. (1998). Aerogels—Airy Materials: Chemistry, Structure, and Properties. *Angewandte Chemie International Edition*, 37(1–2), 22–45.
- Hareid, S., Einarsrud, M.-A., & Scherer, G. W. (1994). Mechanical strengthening of TMOS-based alcogels by aging in silane solutions. *Journal of Sol-Gel Science and Technology*, 3(3), 199–204.
- Illera, D., Mesa, J., Gomez, H., & Maury, H. (2018). Cellulose Aerogels for Thermal Insulation in Buildings: Trends and Challenges. *Coatings*, 8(10), 345.
- Jeffrey Brinker, C., & Prakash, S. S. (1999). *Patent No. US 5948482A*.
- Jiménez-Saelices, C., Seantier, B., Grohens, Y., & Capron, I. (2018). Thermal

- Superinsulating Materials Made from Nanofibrillated Cellulose-Stabilized Pickering Emulsions. *ACS Applied Materials & Interfaces*, 10(18), 16193–16202.
- Jimenez, C., Grohens, Y., Cathala, B., & Seantier, B. (2016). *Nano fibrillated cellulose aerogels with thermal superinsulating properties*. (May), 10397.
- Kabbour, H., Baumann, T. F., Satcher, J. H., Saulnier, A., & Ahn, C. C. (2006). Toward new candidates for hydrogen storage: High-surface-area carbon aerogels. *Chemistry of Materials*, 18(26), 6085–6087.
- Kenar, J. A., Eller, F. J., Felker, F. C., Jackson, M. A., & Fanta, G. F. (2014). Starch aerogel beads obtained from inclusion complexes prepared from high amylose starch and sodium palmitate. *Green Chem.*, 16(4), 1921–1930.
- Kistler, S. S. (1931). Coherent expanded aerogels and jellies [5]. *Nature*, 127(3211), 741.
- Koebel, M., Rigacci, A., & Achard, P. (2012). Aerogel-based thermal superinsulation: an overview. *Journal of Sol-Gel Science and Technology*, 63(3), 315–339.
- Koh, H., Le, D., Ng, G., Zhang, X., Phan-Thien, N., Kureemun, U., & Duong, H. (2018). Advanced Recycled Polyethylene Terephthalate Aerogels from Plastic Waste for Acoustic and Thermal Insulation Applications. *Gels*, 4(2), 43.
- Kremer, D. M., Pikal, M. J., Petre, W. J., Shalaev, E. Y., Gatlin, L. A., & Kramer, T. (2009). A procedure to optimize scale-up for the primary drying phase of lyophilization. *Journal of Pharmaceutical Sciences*, 98(1), 307–318.
- Kumar, A., Yadav, N., Bhatt, M., Mishra, N. K., Chaudhary, P., & Singh, R. (2015). Sol-Gel Derived Nanomaterials and It's Applications: A Review. *Research Journal of Chemical Sciences ISSN 2231-606X*, 5(12), 98–105.
- Lee, S., Jeong, M.-J., & Kang, K.-Y. (2015). Preparation of cellulose aerogels as a nano-biomaterial from lignocellulosic biomass. *Journal of the Korean Physical Society*, 67(4), 738–741.
- Li, J., Lei, Y., Xu, D., Liu, F., Li, J., Sun, A., ... Xu, G. (2017). Improved mechanical and thermal insulation properties of monolithic attapulgite nanofiber/silica aerogel composites dried at ambient pressure. *Journal of Sol-Gel Science and Technology*, 82(3), 702–711.
- Li, Y., Grishkewich, N., Liu, L., Wang, C., Tam, K. C., Liu, S., ... Sui, X. (2019). Construction of functional cellulose aerogels via atmospheric drying chemically cross-linked and solvent exchanged cellulose nanofibrils. *Chemical Engineering Journal*, 366(February), 531–538.
- Long, L. Y., Weng, Y. X., & Wang, Y. Z. (2018). Cellulose aerogels: Synthesis,



- applications, and prospects. *Polymers*, 8(6), 1–28.
- Lovskaya, D. D., Lebedev, A. E., & Menshutina, N. V. (2015). Aerogels as drug delivery systems: In vitro and in vivo evaluations. *The Journal of Supercritical Fluids*, 106, 115–121.
- Mackenzie, J. D. (1988). Applications of the sol-gel process. *Journal of Non-Crystalline Solids*, 100(1–3), 162–168.
- Mahadik, D. B., Jung, H.-N.-R., Lee, Y. K., Lee, K.-Y., & Park, H.-H. (2016). Elastic and Superhydrophobic Monolithic Methyltrimethoxysilane-based Silica Aerogels by Two-step Sol-gel Process. *Journal of the Microelectronics and Packaging Society*, 23(1), 35–39.
- Mahadik, D. B., Rao, A. V., Kumar, R., Ingale, S. V., Wagh, P. B., & Gupta, S. C. (2012). Reduction of processing time by mechanical shaking of the ambient pressure dried TEOS based silica aerogel granules. *Journal of Porous Materials*, 19(1), 87–94.
- Maleki, H., Montes, S., Hayati-Roodbari, N., Putz, F., & Huesing, N. (2018). Compressible, Thermally Insulating, and Fire Retardant Aerogels through Self-Assembling Silk Fibroin Biopolymers Inside a Silica Structure—An Approach towards 3D Printing of Aerogels. *ACS Applied Materials & Interfaces*, 10(26), 22718–22730.
- Maningat, C. C., Seib, P. A., Bassi, S. D., Woo, K. S., & Lasater, G. D. (2009). Wheat Starch. In *Starch* (pp. 441–510).
- Markevicius, G., Ladj, R., Niemeyer, P., Budtova, T., & Rigacci, A. (2017). Ambient-dried thermal superinsulating monolithic silica-based aerogels with short cellulosic fibers. *Journal of Materials Science*, 52(4), 2210–2221.
- Nguyen, B. N., Cudjoe, E., Douglas, A., Scheiman, D., McCorkle, L., Meador, M. A. B., & Rowan, S. J. (2016). Polyimide Cellulose Nanocrystal Composite Aerogels. *Macromolecules*, 49(5), 1692–1703.
- Pajonk, G. M. (1998). Transparent silica aerogels. *Journal of Non-Crystalline Solids*, 225, 307–314.
- Patapoff, T. W., & Overcashier, D. E. (2002). The importance of freezing on lyophilization cycle development. *BioPharm*, 15(3), 16-21+72.
- Pekala, R. W., Farmer, J. C., Alviso, C. T., Tran, T. D., Mayer, S. T., Miller, J. M., & Dunn, B. (1998). Carbon aerogels for electrochemical applications. *Journal of Non-Crystalline Solids*, 225(1–3), 74–80.
- Rao, A. P., Rao, A. V., & Pajonk, G. M. (2007). Hydrophobic and physical properties of the ambient pressure dried silica aerogels with sodium silicate precursor using various

- surface modification agents. *Applied Surface Science*, 253(14), 6032–6040.
- Rao, A. V., & Kulkarni, M. M. (2002). Hydrophobic properties of TMOS/TMES-based silica aerogels. *Materials Research Bulletin*, 37(9), 1667–1677.
- Ratti, C. (2012). Freeze-Drying Process Design. In J. Ahmed & M. S. Rahman (Eds.), *Handbook of Food Process Design* (pp. 621–647).
- Scheuerpflug, P., Caps, R., Büttner, D., & Fricke, J. (1985). Apparent thermal conductivity of evacuated SiO<sub>2</sub>-aerogel tiles under variation of radiative boundary conditions. *International Journal of Heat and Mass Transfer*, 28(12), 2299–2306.
- Seantier, B., Bendahou, D., Bendahou, A., Grohens, Y., & Kaddami, H. (2016). Multi-scale cellulose based new bio-aerogel composites with thermal super-insulating and tunable mechanical properties. *Carbohydrate Polymers*, 138, 335–348.
- Sehaqui, H., Zimmermann, T., & Tingaut, P. (2014). Hydrophobic cellulose nanopaper through a mild esterification procedure. *Cellulose*, 21(1), 367–382.
- Simón-Herrero, C., Caminero-Huertas, S., Romero, A., Valverde, J. L., & Sánchez-Silva, L. (2016). Effects of freeze-drying conditions on aerogel properties. *Journal of Materials Science*, 51(19), 8977–8985.
- Soleimani Dorcheh, A., & Abbasi, M. H. (2008). Silica aerogel; synthesis, properties and characterization. *Journal of Materials Processing Technology*, 199(1), 10–26.
- Sun, T., Zhuo, Q., Liu, X., Sun, Z., Wu, Z., & Fan, H. (2014). Hydrophobic silica aerogel reinforced with carbon nanotube for oils removal. *Journal of Porous Materials*, 21(6), 967–973.
- Trache, D., Hussin, M. H., Hui Chuin, C. T., Sabar, S., Fazita, M. R. N., Taiwo, O. F. A., ... Haafiz, M. K. M. (2016). Microcrystalline cellulose: Isolation, characterization and bio-composites application—A review. *International Journal of Biological Macromolecules*, 93, 789–804.
- Ubeyitogullari, A., Brahma, S., Rose, D. J., & Ciftci, O. N. (2018). In Vitro Digestibility of Nanoporous Wheat Starch Aerogels. *Journal of Agricultural and Food Chemistry*, 66(36), 9490–9497.
- Ubeyitogullari, A., & Ciftci, O. N. (2016). Formation of nanoporous aerogels from wheat starch. *Carbohydrate Polymers*, 147, 125–132.
- Ulker, Z., & Erkey, C. (2014). An emerging platform for drug delivery: Aerogel based systems. *Journal of Controlled Release*, 177, 51–63.
- Wagh, P. B., & Ingale, S. V. (2002). Comparison of some physico-chemical properties of hydrophilic and hydrophobic silica aerogels. *Ceramics International*, 28(1), 43–50.

- Wang, B., Zhang, W., Zhang, W., Mujumdar, A. S., & Huang, L. (2005). Progress in Drying Technology for Nanomaterials. *Drying Technology*, 23(1–2), 7–32.
- Wang, L.-J., Zhao, S.-Y., & Yang, M. (2009). Structural characteristics and thermal conductivity of ambient pressure dried silica aerogels with one-step solvent exchange/surface modification. *Materials Chemistry and Physics*, 113(1), 485–490.
- Wang, Y., Wu, K., Xiao, M., Riffat, S. B., Su, Y., & Jiang, F. (2018). Thermal conductivity, structure and mechanical properties of konjac glucomannan/starch based aerogel strengthened by wheat straw. *Carbohydrate Polymers*, 197, 284–291.
- Woignier, T., Hafidi Alaoui, A., Primera, J., & Phalippou, J. (2009). Mechanical properties of aerogels: Brittle or plastic solids? *Key Engineering Materials*, 391, 27–44.
- Wu, S., Du, A., Huang, S., Sun, W., Xiang, Y., & Zhou, B. (2016). Solution-processable polyimide aerogels with high hydrophobicity. *Materials Letters*, 176, 118–121.
- Yan, L., Ren, H., Zhu, J., Bi, Y., & Zhang, L. (2019). One-step eco-friendly fabrication of classically monolithic silica aerogels via water solvent system and ambient pressure drying. *Journal of Porous Materials*, 26(3), 785–791.
- Yang, J., Zhang, E., Li, X., Zhang, Y., Qu, J., & Yu, Z.-Z. (2016). Cellulose/graphene aerogel supported phase change composites with high thermal conductivity and good shape stability for thermal energy storage. *Carbon*, 98, 50–57.
- Zaman, A., Huang, F., Jiang, M., Wei, W., & Zhou, Z. (2019). Preparation, Properties, and Applications of Natural Cellulosic Aerogels: A Review. *Energy and Built Environment*, 0–40.
- Zamora-Sequeira, R., Ardao, I., Starbird, R., & García-González, C. A. (2018). Conductive nanostructured materials based on poly-(3,4-ethylenedioxythiophene) (PEDOT) and starch/ $\kappa$ -carrageenan for biomedical applications. *Carbohydrate Polymers*, 189, 304–312.
- Zhai, S., Su, H., Taylor, R., & Slater, N. K. H. (2005). Pure ice sublimation within vials in a laboratory lyophiliser; comparison of theory with experiment. *Chemical Engineering Science*, 60(4), 1167–1176.
- Zhang, Y., Zhu, J., Ren, H., Bi, Y., Shi, X., Wang, B., & Zhang, L. (2017). A novel starch-enhanced melamine-formaldehyde aerogel with low volume shrinkage and high toughness. *Journal of Porous Materials*, 24(5), 1303–1307.
- Zhao, S., Malfait, W. J., Demilecamps, A., Zhang, Y., Brunner, S., Huber, L., ... Koebel, M. M. (2015). Strong, Thermally Superinsulating Biopolymer-Silica Aerogel Hybrids by Cogelation of Silicic Acid with Pectin. *Angewandte Chemie*, 127(48), 14490–

14494.

Zhu, F. (2019). Starch based aerogels: Production, properties and applications. *Trends in Food Science and Technology*, 89(April), 1–10.